NASA TECHNICAL NOTE

NASA TN D-3570

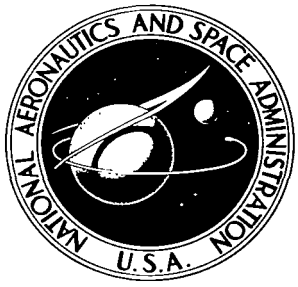

NASA TN D-3570

LANDING CHARACTERISTICS OF A DYNAMIC MODEL OF THE HL-10 MANNED LIFTING ENTRY VEHICLE

by Sandy M. Stubbs

Langley Research Center
Langley Station, Hampton, Va.

NATIONAL AERONAUTICS AND SPACE ADMINISTRATION • WASHINGTON, D. C. • NOVEMBER 1966

NASA TN D-3570

LANDING CHARACTERISTICS OF A DYNAMIC MODEL OF THE HL-10 MANNED LIFTING ENTRY VEHICLE

By Sandy M. Stubbs

Langley Research Center
Langley Station, Hampton, Va.

Technical Film Supplement L-916 available on request.

NATIONAL AERONAUTICS AND SPACE ADMINISTRATION

For sale by the Clearinghouse for Federal Scientific and Technical Information
Springfield, Virginia 22151 – Price $2.50

LANDING CHARACTERISTICS OF A DYNAMIC MODEL OF THE HL-10 MANNED LIFTING ENTRY VEHICLE

By Sandy M. Stubbs
Langley Research Center

SUMMARY

Several tricycle landing-gear configurations, all of which used two main rear skids with variations in the nose gear, were investigated to determine landing accelerations and slideout stability for horizontal type landings. Techniques for counteracting side wind or sloping (crowned) runway forces which might cause the spacecraft to slide off the runway were also investigated. A free-swiveling nose-wheel configuration, with and without a roll-steering system, a torque-steering configuration, and a nose-skid configuration were investigated for landing conditions consistent with the winged entry type spacecraft.

A basic configuration without a landing gear was investigated to determine its accelerations and stability in a skid-rocker (belly) type landing. The vehicle was landed on a runway landing surface with and without a braking parachute. Calm-water landings were investigated in both horizontal (aircraft type) and vertical (parachute type) landing modes. Parachute type landings were also made in waves.

Results indicate that the vehicle with the tricycle landing-gear configurations, using either the free-swiveling nose wheel or the nose-skid configuration has good tracking characteristics for landings without the presence of a side wind or a crowned runway. The roll-steering or the torque-steering concepts can be used to obtain tracking control when side winds and crowned runways are present. Roll steering and torque steering have the feature that either one can be used by the pilot with less danger of oversteering than with conventional mechanical steering methods. This feature results because a constant side force is provided from roll and torque steering which is independent of the spacecraft yaw attitude.

The slideout stability for the basic configuration in a skid-rocker type landing on a runway surface was unsatisfactory. The basic configuration without landing gear when landed on calm water in a horizontal landing mode resulted in violent motions after first impact. Satisfactory results were obtained for vertical-type water landings.

INTRODUCTION

Considerable interest has been shown in manned lifting entry vehicles capable of horizontal landings because their large landing footprint capability enables them to make power-off landings on existing 10,000 ft (3000 m) runways. Several different lifting entry vehicles have evolved from aerodynamic testing and it was desirable to investigate the landing characteristics (impact accelerations and slideout stability) of a spacecraft of this type. A summary of a lifting entry vehicle study is presented in reference 1.

Because of touchdown-point errors generally associated with unpowered landings at high speed, it is desirable to reduce slideout (landing run) distance to a minimum. A previous investigation of an all-skid tricycle landing gear is reported in reference 2. As stated in reference 2, a skid system was chosen because it has high friction drag, low weight, and simplicity. The vehicle used in the referenced investigation was designed primarily for lake-bed-type landings in which the vehicle could be landed into the wind. It was directionally stable but could produce no side force to counter runway crown or cross winds. There is a good possibility that runway cross winds will exist that could force the vehicle off the runway if a nonsteerable skid-type landing gear is used. Crown or sloping runways might also cause the vehicle to slide off the runway. The use of skids, therefore, produces a tracking control problem under these conditions. In order to keep the spacecraft on the runway in the presence of cross winds or runway crown, a method of creating a controllable side force is necessary. Conventional steering methods of turning the nose wheel are not satisfactory in that they require a high degree of pilot skill to keep from oversteering and possibly getting into an uncontrolled skid.

The purpose of the present paper was to investigate hard-surface and water landings of various configurations of a dynamic model of an early version of the HL-10 spacecraft to determine the characteristics of each configuration. Four configurations were investigated; three for hard-surface landings only and one for both hard-surface and water landings. The three hard-surface landing configurations had two rear main skids in conjunction with a free-swiveling nose wheel, a torque-steering nose wheel, and a nose skid. Two methods, a torque-steering concept (ref. 3) and a roll-steering concept, capable of producing a constant side force regardless of yaw attitude when a nose wheel is employed, were investigated for hard-surface landings. The fourth configuration (basic configuration) was used with and without a braking parachute as a skid rocker (belly landing) for hard-surface landings and also in water landings. Previous skid-rocker investigations (see refs. 4, 5, and 6) indicate that landing accelerations are reasonable but stability during slideout can present problems. Water landings were considered for emergency landings and both horizontal (airplane type) and vertical (parachute type) landings were studied.

Impact accelerations were obtained and dynamic behavior was recorded by motion-picture photography (Film supplement L-916). The investigation was conducted in the Langley impacting structures facility.

The units used for the physical quantities defined in this paper are given both in the U.S. Customary Units and in the International System of Units (SI) (ref. 7). Appendix A presents factors relating these two systems of units.

DESCRIPTION OF MODEL

The model used in the investigation was a 1/11-scale dynamic model of an early version of the HL-10 spacecraft. Dimensions of the model with a tricycle landing gear are shown in figure 1. The model was formed from a solid piece of balsa wood and then covered with a 1/32-in. (0.8-mm) thickness of glass fiber. A hole was cut in the top of the model at the center of gravity and hardwood blocks were glued in place to serve as accelerometer mounts. The scale relationships used in the investigation are shown in table I.

Tricycle Landing-Gear Configurations

Several configurations using a tricycle landing gear were investigated using the model shown in figure 1. The pertinent parameters of mass, moment of inertia, and size of the spacecraft are given in table II. Photographs of this configuration are shown in figure 2.

Details of the tricycle landing-gear assemblies are shown in figure 3. Figure 3(a) shows details of the rear main landing-gear strut and skid attached to the model with the model at 0° pitch attitude. The skid material used in the model investigation was aluminum. All landing gears used shock-absorbing energy straps to attenuate the landing impact. The model energy strap was made of low carbon nickel wire. Landing loads imposed on the gear strut were absorbed in tension by the energy strap. The load exceeded the yield strength of the strap and it elongated during the strut stroke. Stress-strain characteristics of a sample of the model energy strap material are shown in figure 4. When the strap yielded in tension, it allowed the strut to pivot and stroke up to 1.40 in. (3.6 cm) (model scale).

Details of the nose-wheel assembly used on the free-swiveling nose-wheel configuration are shown in figure 3(b). A parallel linkage was used to allow the nose-wheel assembly to stroke up to 0.9 in. (2.3 cm) (model scale). The nose wheel was made of solid rubber and attached to the parallel linkage in a trailing position.

For the torque-steering configuration, a stop was used to keep the nose wheel in a straight-ahead position until the landing impact occurred. At impact, the nose gear

stroked, freed itself from the stop, and thus was allowed to swivel, torque being applied about the swivel axis using a piece of shock cord (fig. 2(b)).

Details of the nose-skid assembly are shown in figure 3(c). The skid has a "dishpan" shape and the sliding surface was covered with Teflon to reduce friction. The skid was attached to the strut with a universal joint to allow it to rest flat against the landing surface regardless of vehicle pitch or roll. Stops were used to limit the movement of the skid.

Basic Configuration

Several different types of landings were investigated by using the basic configuration in a skid-rocker or "belly" landing. The skid-rocker shape was that of the bottom of the HL-10 model without landing gear of any type. Figure 5(a) is a photograph of the basic configuration. Figure 5(b) shows the model on the launch apparatus and figure 5(c) shows the braking parachute used to stabilize the model and reduce the landing slideout distance. Two shock-absorbing tabs (fig. 6) were used on the aft end of the model. The tabs were made of aluminum and were designed to yield in bending to make a smooth transition from sink speed to angular velocity and also to absorb some of the energy due to the vertical velocity. The purpose of the skid-rocker concept is to convert sink speed at touchdown to angular velocity in pitch or rocking and let damping forces dissipate the energy of the vertical component of velocity while the energy due to horizontal velocity is dissipated by friction as the vehicle slides to a stop.

The braking parachute used with the skid-rocker configuration was approximately 24 in. (0.6 m) diameter (model scale) in the flat condition. A bridle and riser system was used to attach the parachute to the model. The parachute trailed the model by approximately four fuselage lengths.

APPARATUS AND PROCEDURE

The instrumentation used in the investigation consisted of strain-gage accelerometers connected by a trailing cable to a control panel with power supply, and an oscillograph. The accelerometer characteristics are presented in table III. Motion pictures were taken to record dynamic behavior of the model. Figure 7 shows the model acceleration axes, landing attitude, and flight path. The apparatus used to launch the tricycle landing-gear configuration was a monorail launcher shown in figures 5(b) and 8. The model was attached to the carriage which in turn was attached to a continuous cable pulled by an electric motor.

Tricycle Landing-Gear Configurations

During hard-surface landings with the tricycle landing-gear configurations, the model was launched as a free body onto a plywood runway surface 200 ft (61 m) long and 13.6 ft (4.1 m) wide. This surface represented a full-scale length of 2200 ft (670 m) and a width of 150 ft (46 m). The coefficient of friction of the model with two rear aluminum skids and a nose wheel on the plywood runway was approximately 0.4. All tests of the tricycle landing-gear configurations used the same rear landing-gear skids. The landing tests were made at a pitch attitude of 25°. Yaw angles of 0° and 10° were investigated and the vertical or sink speed was approximately 3 ft/sec (0.9 m/s) model scale. Slideout tests were made to study steering concepts when it was determined that the landing impact introduced random variables of vehicle pitch and roll during slideout because of uneven stroking of the landing gear. For slideout tests, the landing gear was locked to prevent stroking and thus maintain vehicle attitude during slideout. The model scale vertical velocity at touchdown was reduced to approximately 0.6 ft/sec (0.2 m/s) and the pitch attitude was 0°.

Free-swiveling nose-wheel configuration.- The free-swiveling nose-wheel configuration was investigated to have a base to compare the effectiveness of the torque-steering and roll-steering concepts. The free-swiveling nose wheel had limiters on the nose wheel that kept it from swiveling more than $\pm 45^{\circ}$ from the longitudinal axis of the vehicle. Since the accelerations were expected to be at or near the same values for all the tricycle landing-gear configurations, they were measured only during the free-swiveling nose-wheel tests.

The roll-steering concept was investigated with the free-swiveling nose-wheel configuration. The vehicle, in an attempt to produce a side force, was purposely rolled from 0° to 10° right or left by locking the rear landing gear to simulate unsymmetrical stroking. It was assumed that the pilot could control the rolled attitude from 0° to 10° by a hydraulic jacking arrangement in which one of the rear landing gear would be extended or retracted a small amount from the normal runout position. Because of the trail of the nose wheel, the rolled spacecraft can produce a side force. This condition is similar to riding a bicycle without holding the handle bars. When the bicycle is leaned (rolled) to the left, the front wheel turns to the left, and thus creates a side force to the left which changes the direction of motion. When the wind is blowing from the left, a slight roll to the left is necessary to create the side force needed to travel straight along a roadway. A sketch showing the forces on the tricycle landing gear for a left roll condition is shown in figure 9. The yawing moments about the vehicle center of gravity produced by these forces are also shown. The rear skids produce only a drag force and the nose wheel produces a drag force and a side force. The vehicle will seek the yaw attitude in which the moments about the vehicle center of gravity produced by the landing gear are in equilibrium. In the equilibrium condition the clockwise moment produced by the right

rear skid will be balanced by counterclockwise moments produced by the left rear skid and the nose wheel. When this condition occurs, the drag forces are acting to stop the vehicle and the side force produced only by the nose wheel acts in a direction to counteract the wind force.

Torque-steering nose-wheel configuration.- The torque-steering concept was investigated by using the free-swiveling nose-wheel configuration with torque applied to the nose wheel. The amount of torque could be varied from one run to the next, but once it was set for a given run it remained essentially constant throughout the run.

The forces and dynamics encountered by using the torque-steering concept are similar to those experienced in the roll-steering concept. The difference in the two concepts is in the control of the nose wheel to produce a side force. The constant torque was applied by using a shock cord attached to a torque arm shown in figures 2(b) and 3(b). The torque was varied by positioning the shock chord various distances out on the torque arm.

Nose-skid configuration.- The nose-skid investigation was conducted by using the two rear skids of the previous configurations in conjunction with a nose-skid strut arrangement. Details of the "dishpan" type nose skid and strut are shown in figure 3(c). The purpose of this investigation was to determine the effect of a nose skid on slideout stability of a rolled spacecraft. The roll attitudes investigated ranged from 0° to 10°.

Basic Configuration

Landing on hard surface.- The basic configuration was landed on a plywood runway surface at pitch attitudes of 15°, 20°, and 25° to determine its skid-rocker landing characteristics. The primary landing attitude was chosen as 15° because the bottom curvature of the vehicle at this attitude was tangent to the runway surface. (See fig. 10.) The horizontal landing velocity of the spacecraft is approximately 400 ft/sec (120 m/s) (full scale) at an attitude of 15°. The launch apparatus was limited to approximately 100 ft/sec (30 m/s) model scale or about 330 ft/sec (100 m/s) full scale; thus, this part of the investigation (15° landing attitude) was made at speeds less than those necessary to fly the vehicle. It was considered, however, that the rocking motion and slideout characteristics could be adequately studied at this test speed. Because of the high horizontal landing speed at an attitude of 15° and the coefficient of friction of the glass fiber model on the wood runway of 0.35 to 0.45, the length of the runway was inadequate to allow the vehicle to slide to a stop. An arresting net was used to stop the vehicle at the end of the runway.

A braking parachute was used for some of the skid-rocker landings in an effort to increase directional stability, reduce slideout distance, and give better slideout dynamics in general. The parachute was packaged in a container mounted on the launch carriage. As the model left the launch carriage it started pulling the parachute out of the container.

By the time the vehicle had traveled about 5 fuselage lengths the braking parachute was fully opened. The braking parachute was not optimized for this investigation and a pulsating effect was evident. The braking parachute was used for all runway landings of the skid-rocker configuration in which acceleration data were obtained.

Horizontal landings on water.- Horizontal water landings were made with the same launch apparatus used for runway landings. Figure 8(b) is a photograph showing the runway surface removed for water landings. Full-scale horizontal velocities ranged from 250 ft/sec (76 m/s) to 110 ft/sec (33.5 m/s). The sink speed at impact was about 10 ft/sec (3.0 m/s) full scale and the landing attitude was 25°. The vehicle was landed without a landing gear, and with and without the braking parachute.

Vertical landings on water.- Vertical parachute type landings were made in calm water and in waves. Full-scale vertical velocities from 40 to 60 ft/sec (12 to 18 m/s) were investigated at zero horizontal velocity at landing attitudes from 80° to 100° (tail first) and -70° to -90° (nose first). Only the positive landing attitude range was tested for landings in waves. The waves used in the investigation were 5.5 ft (1.7 m) high and 209 ft (64 m) long (full scale) crest to crest.

RESULTS AND DISCUSSION

A short motion-picture film supplement of typical hard-surface and water landings is available on loan from the NASA. A request card and a description of the film will be found at the end of this paper. All data presented in this section are converted to full-scale values by use of the scale relations given in table I.

Tricycle Landing-Gear Configurations

A summary of results of runway landings using the tricycle landing-gear configurations is presented in table IV. A summary of slideout tests on the same configurations is presented in table V.

Free-swiveling nose-wheel configuration.- Acceleration data for the tricycle landing-gear configuration using the free-swiveling nose wheel for landings on a plywood runway at a 25° landing attitude are shown in table VI. Normal acceleration values ranged from 4.6g to 5.6g and longitudinal accelerations were from 1.1g to 1.4g. Acceleration data for the other configurations of the tricycle landing-gear investigation were considered to be at or near the same low values as those obtained with the free-swiveling nose wheel and no acceleration data were obtained for the other configurations. Typical oscillograph records obtained by using the free-swiveling nose wheel are shown in figure 11. The rear skids were first to contact the runway and generally produced the maximum normal acceleration. The nose gear then contacted the runway and at this time the

maximum longitudinal acceleration occurred. When the nose gear impacted the runway, the rear skids were very lightly loaded and lifted off the runway surface. This effect can be seen in figure 12. For a short period of time, the vehicle was balanced on the nose wheel. The rear of the vehicle then came back down, the rear skids made contact a second time, and a smooth slideout followed.

The free-swiveling nose wheel used on the tricycle landing-gear configuration was a very stable arrangement. The rear skids with the much higher drag forces tended to keep the longitudinal axis of the vehicle lined up with the runway. Little drift was noted to either side of the runway center line. If a side wind were present or if the runway were sloped down from the center to the sides (crown), the vehicle could be expected to drift laterally to the side of the runway, and perhaps, even off the runway.

Because of the inability of the free-swiveling nose-wheel configuration to develop side forces, the roll-steering concept was investigated. Figure 13 shows the effect of roll steering on the spacecraft for slideout tests at an impact attitude of 0^{o}. The roll attitude in figure 13(a) is 0^{o}. The model was landed just to the left of the runway center stripe and drifted slightly to the left (approximately 11 ft (3.4 m)) full scale. The runout was essentially straight. The black stripe on the runway at the right side of the photograph (left side of the model) indicates where the edge of a 150 ft (46 m) wide full-scale runway would be. (See fig. 13(a), photograph 1.) Figure 13(b) shows a landing with 5^{o} left roll during slideout. A displacement to the left which actually carries the vehicle off the runway (across black stripe) indicates an ability of roll steering to induce a lateral force. Therefore, for a specific side wind condition, this induced lateral force would be expected to result in a straight runout similar to the no-wind 0^{o} roll case (fig. 13(a)). If the roll attitude is increased to 10^{o} left (fig. 13(c)), the side force is excessive and causes a 90^{o} left yaw and the ensuing turnover. Conventional steering methods of turning the nose wheel are not satisfactory in that they require a high degree of pilot skill to keep from oversteering and possibly getting into an uncontrolled skid. The roll steering produces a constant side force regardless of the spacecraft yaw attitude and could possibly be applied by the pilot with less danger of oversteering.

Torque-steering nose-wheel configuration.- The effect of the torque steering is illustrated in figure 14. Figure 14(a) shows a landing with no torque being applied. The model was landed just to the left of the runway center stripe and drifted slightly to the left (approximately 11 ft (3.4 m)) full scale. The runout was essentially straight. Figure 14(b) shows a landing with 360 ft-lb (488 m-N) of left torque being applied. A displacement to the left which actually carries the vehicle off the runway (across black stripe) indicates an ability of the torque steering to induce a lateral force.

Figures 14(c) and 14(d) illustrate the effect of increasing torque with the vehicle sliding off the runway earlier in the runout. These torque conditions would balance out

respectively larger wind forces. Figure 14(e) shows what could happen if too much torque is applied. In this landing 1029 ft-lb (1395 m-N) of left torque is applied to the nose wheel. The friction force between the runway and the nose wheel is great enough that the vehicle yaws to the left sufficiently to produce an overturning right roll. In comparison with conventional steering, the torque steering produces a constant side force regardless of the vehicle yaw attitude and could possibly be applied by the pilot with less danger of oversteering.

A typical sequence of photographs showing the control effectiveness of torque steering opposing side forces produced by unanticipated roll attitudes of the spacecraft is shown in figure 15. The vehicle is rolled right 5° simulating unsymmetrical stroking of the rear landing gear. It is assumed here that no roll steering is provided and that the vehicle inadvertently attained a roll attitude for slideout. The vehicle without torque steering drifted to its right into the net bordering the edge of the runway. (See table V for a right roll condition of 5°.) With a left torque of 514 ft-lb (697 m-N) applied the vehicle drifted right only 15 ft (4.6 m) full scale. At the end of the runout, the vehicle made a gentle turn to the left.

Nose-skid configuration.- Figure 16 shows a typical sequence using the nose-skid gear and a roll attitude of 5° left. The vehicle slides straight along the runway; thus no side force was developed by roll when the nose skid was used. Since no side force is produced, side winds or runway crown would cause this configuration to drift laterally and perhaps run off the runway edge. At a 10° left roll the nose-skid configuration rolled over on its side. This condition is due to the geometry of the nose gear and at 10° roll displaces the "dishpan" skid laterally outboard from the longitudinal axis through the center of gravity. The vehicle will barely sit upright at this attitude when at rest and during the slideout test, turnover occurred immediately on touchdown.

Basic Configuration

Landings on hard surface.- Because of aerodynamic requirements the bottom surface of the HL-10 model did not have the optimum curvature for a skid-rocker landing but was nevertheless used to determine its skid-rocker landing characteristics.

A typical oscillograph record of the basic configuration in a skid-rocker landing on a plywood runway is shown in figure 17. The initial peak on the normal acceleration trace indicates when the shock-absorbing tab strikes the runway and the sharp spike that follows indicates the vehicle undersurface striking the runway. The faired acceleration, shown as a dashed line during the first major rocking acceleration, reached a maximum value of 9.5g. Between the first and second major rocking accelerations, the model rotated in pitch and bumped along the runway, as is indicated by the acceleration spikes between the two major rocking accelerations. The results of drag from sliding friction and the

braking parachute can be seen on the longitudinal acceleration trace. Drag from the braking parachute gives approximately 2g acceleration.

Acceleration data presented in table VII and figure 18 were obtained from fairings of oscillograph records made during skid-rocker landings with the braking parachute on a plywood runway. Landings were made with and without the shock-absorbing tab (fig. 6). Results with and without the tab are very similar. See table VII. Normal acceleration curves for runs made using the shock-absorbing tab are shown in figure 18. The lowest normal acceleration occurred at a landing attitude of 20° and a horizontal velocity of 250 ft/sec (76 m/s).

The runout behavior of the vehicle was very violent in skid-rocker landings without the braking parachute. Only the landing attitude of 15° was tested without the braking parachute. The vehicle bounced along the runway both up and down and in a rolling or walking motion from side to side. The vehicle generally yawed, either right or left and occasionally as much as 90°. The vehicle drifted to the side sometimes more than 75 ft (23 m) (full scale) and this drifting indicated that it would have run off the edge of a 150 ft (46 m) runway. The velocity was still very high by the time the vehicle reached the end of the runway and it was necessary to arrest the vehicle by catching it in a net.

The braking parachute improved tracking and directional stability appreciably. The parachute and its attachments were not optimized and often the parachute would be trailing in a lateral offset and would cause the vehicle to yaw. This condition had a slightly detrimental effect on directional stability. With the braking parachute, the vehicle always stopped before it ran off the end of the runway and at no time did the parachute allow the vehicle to drift laterally as much as 75 ft (23 m). The parachute reduced the bouncing motions, and, in general, slideout behavior was much improved over runs made without the braking parachute.

Horizontal landings on water.- Typical oscillograph records for horizontal-type calm-water landings are shown in figure 19. For the typical run shown, the first impact reached a maximum normal acceleration of 7g, the second impact was approximately 6.4g, and at the third impact the vehicle hit in an inverted attitude and accelerations of -10.3g were experienced. Acceleration data for horizontal-type water landings are presented in table VIII. Accelerations for the first impact are in close agreement, but for the second and third impacts the band of scatter increases. This scatter is due to widely varying vehicle attitudes during the second and third impacts.

A typical sequence of events for high-velocity calm-water landings with the HL-10 vehicle starts when the aft portion of the vehicle strikes the water and a suction force on the tail initiates a positive pitch motion. This positive pitch causes the vehicle to fly out of the water. The second and/or third impacts generally were very unpredictable, the vehicle striking at high positive or even negative pitch angles or in an inverted attitude.

The vehicle occasionally dived on second or third impact. The vehicle always came to rest in an abrupt fashion on the second or third impacts in either an inverted or right-side-up attitude.

The braking parachute was investigated briefly in horizontal water landings in an attempt to stabilize the vehicle and to reduce the horizontal velocity. The parachute tended to stabilize the vehicle but was far from adequate in this respect. The results with and without the parachute were very similar.

Lower horizontal velocities were investigated without use of the braking parachute to determine a satisfactory calm-water landing speed for the HL-10 vehicle. Horizontal velocities at the 25° landing attitude were reduced from 255 ft/sec (78 m/s) to 150 ft/sec (46 m/s) and subsequently to 110 ft/sec (34 m/s) before suitable landing dynamics were obtained.

Vertical landings on water.- A photograph of the vehicle landing in calm water is shown in figure 20. Typical oscillograph records of vertical-type water landings at simulated parachute letdown conditions are shown in figure 21. For the 90° landing attitude or tail-first impact, the maximum longitudinal acceleration at impact was -3.8g. The -3.8g acceleration is a transient spike of short duration and is caused by the blunt trailing edge of the vehicle. A sustained acceleration, following the spike, reaches a magnitude of approximately -2.6g. For the -90° landing attitude or nose-first impact, the maximum longitudinal acceleration was approximately 3.8g. The entry into the water with the rounded nose surface was smooth and no transient spike occurred. The maximum normal acceleration on the second impact is -6.6g, the negative sign indicating that the vehicle hit in an inverted position.

Accelerations are given in table IX for both first and second impacts for the normal acceleration and the spike or transient acceleration as well as the sustained values for first-impact longitudinal acceleration. The longitudinal acceleration on the second impact was always very small.

Sustained longitudinal accelerations and first-impact normal accelerations are plotted in figure 22 for various landing attitudes. The solid symbols indicate that the vehicle came to rest in an inverted position. The longitudinal accelerations varied from 4g at a -90° attitude to -2.8g at a 95° attitude. For the range of attitudes tested, the first-impact normal acceleration varied from 0.5g at -90° to 3g at -70° and from -0.8g at 100° to 2g at 80°.

The effect of increasing vertical velocity on longitudinal and normal accelerations is shown in figure 23. The data plotted are for $\pm 85^{\circ}$ landing attitudes. The sustained longitudinal acceleration at the -85° attitude varied from 3.2g at a vertical velocity of 40 ft/sec (12 m/s) to 3.9g at 60 ft/sec (18 m/s). The sustained longitudinal acceleration at the 85° attitude varied from -2.4g to -2.6g. The first-impact normal accelerations

were less than 2g for the vertical velocity range. The small increases in longitudinal and normal acceleration, for the angles of the tests, indicate that a higher impact velocity might be feasible for the HL-10 type spacecraft which could result in a letdown parachute weight saving. The water penetration is greater, however, with higher impact velocities and thus the hydrostatic pressure on the submerged vehicle structure is greater and could pose an offsetting weight penalty.

The data shown in figure 22 indicate whether the basic configuration came to rest inverted or right side up. For all runs, the vehicle entered the water with a smooth motion. For landing attitudes near $\pm 90^{\circ}$, the vehicle was almost completely submerged before the vertical velocity was dissipated. The vehicle then rose and because of its buoyancy characteristics gained sufficient velocity to rise clear of the water surface. The vehicle then fell back for a second impact in the water. For runs at angles less than $\pm 85^{\circ}$, the vehicle entered the water with a pitching motion that tended to bring it to a horizontal pitch attitude. The penetration was not as great and the vehicle rose to the surface in a smooth manner with no second impact. Landing attitudes of 95° and greater resulted in the vehicle coming to rest in an inverted position. Landing attitudes of -90° also resulted in the vehicle coming to rest in an inverted position. For landing attitudes less than $\pm 90^{\circ}$, all runs were stable (vehicle came to rest right side up).

Landings made in waves 5.5 ft (1.7 m) high and 209 ft (64 m) long (full scale) to determine the stability characteristics when water motion is involved gave the same results as those obtained in calm water.

CONCLUDING REMARKS

Several tricycle landing-gear configurations were investigated by using a 1/11-scale dynamic model of an early version of the HL-10 spacecraft. A free-swiveling nose-wheel configuration with and without roll steering, a torque-steering configuration, and a nose-skid configuration all using two main rear skids, were tested. Runway-type landings using the tricycle landing gear resulted in maximum normal and longitudinal accelerations of approximately 5.6g and 1.4g, respectively. The tricycle landing-gear configurations using either the free-swiveling nose wheel or the nose skid resulted in good tracking characteristics for landings without the presence of side wind or runway crown. The roll-steering or the torque-steering concepts can be used to obtain tracking control when side winds and crowned runways are present. Roll steering and torque steering have the feature that either one can be applied by the pilot with less danger of oversteering than with conventional mechanical steering methods. This feature results because a constant side force is provided from roll or torque steering which is independent of the spacecraft yaw attitude.

The basic configuration when landed as a skid rocker (belly landing) on a runway surface gave maximum normal accelerations of approximately 12g at a landing attitude of 20°. The maximum longitudinal accelerations were 6.8g for all attitudes tested. The slideout dynamics for the skid-rocker landings were erratic and often the vehicle would slide off the side of a 150 ft (46 m) wide (full scale) runway. A braking parachute improved the directional and tracking stability and shortened the slideout distance.

The basic configuration, when landed in calm water in a horizontal landing mode, gave normal accelerations on first impact of about 7g. After the first impact violent motions were encountered. Parachute-type (vertical landings) gave sustained longitudinal accelerations of approximately 3.9g and at landing attitudes less than $\pm 85^{\circ}$, motions of the vehicle were smooth. Parachute-type landings in waves were very similar to calm-water landings.

Langley Research Center,
National Aeronautics and Space Administration,
Langley Station, Hampton, Va., July 11, 1966.

APPENDIX A

CONVERSION OF U.S. CUSTOMARY UNITS TO SI UNITS

The International System of Units (SI) was adopted by the Eleventh General Conference on Weights and Measures, Paris, October 1960, in Resolution No. 12 (ref. 7). Conversion factors for the units used herein are given in the following table:

Physical quantity	U.S. Customary Unit	Conversion factor (*)	SI Unit
Length	in.	0.0254	meters (m)
Area	in^2	6.4516×10^4	$meters^2$ (m^2)
Mass	slug	14.59339	kilograms (kg)
Moment of inertia	$slug\text{-}ft^2$	1.35582	$kilograms\text{-}meters^2$ ($kg\text{-}m^2$)
Velocity	ft/sec	0.3048	meters/second (m/s)
Linear acceleration	ft/sec^2	0.3048	$meters/second^2$ (m/s^2)
Force	lbf	4.448	newtons (N)
Stress	lbf/in^2	6.89×10^3	$newtons/meter^2$ (N/m^2)
Torque	ft-lbf	1.355828	meter-newton (m-N)

*Multiply value given in U.S. Customary Unit by conversion factor to obtain equivalent value in SI Unit.

REFERENCES

1. Rainey, Robert W.: Summary of an Advanced Manned Lifting Entry Vehicle Study. NASA TM X-1159, 1965.

2. Blanchard, Ulysse J.: Landing Characteristics of a Winged Reentry Vehicle With All-Skid Landing Gear Having Yielding-Metal Shock Absorbers. NASA TN D-1496, 1962.

3. Joyner, U. T.: Nose Gear Steering System for Vehicle With Main Skids. U.S. Patent Office No. 3,208,694, Sept. 28, 1965.

4. Blanchard, Ulysse J.: Landing Characteristics of a Lenticular-Shaped Reentry Vehicle. NASA TN D-940, 1961.

5. Stubbs, Sandy M.: Investigation of the Skid-Rocker Landing Characteristics of Spacecraft Models. NASA TN D-1624, 1963.

6. Mayo, Wilbur L.: Skid Landings of Airplanes on Rocker-Type Fuselages. NASA TN D-760, 1961.

7. Mechtly, E. A.: The International System of Units – Physical Constants and Conversion Factors. NASA SP-7012, 1964.

TABLE I.- SCALE RELATIONSHIPS

[λ, scale of model = 1/11]

Quantity	Full-scale value	Scale factor	Model
Dynamic model:			
Length	l	λ	λl
Area	A	λ^2	$\lambda^2 A$
Mass	m	λ^3	$\lambda^3 m$
Moment of inertia	I	λ^5	$\lambda^5 I$
Time	t	$\sqrt{\lambda}$	$\sqrt{\lambda} t$
Speed	v	$\sqrt{\lambda}$	$\sqrt{\lambda} v$
Linear acceleration	a	1	a
Force	F	λ^3	$\lambda^3 F$
Energy strap:			
Unit stress	σ	1	σ
Cross-sectional area*	A	λ^3	$\lambda^3 A$
Force	F	λ^3	$\lambda^3 F$

*For dynamic similarity it is convenient to keep linear accelerations 1:1 for model and full scale. Since the mass varies as the cube of the scale factor (λ^3), all applied forces must be varied by the same factor. A geometrically scaled energy strap would vary as λ^2; therefore, it is necessary to distort the cross-sectional area of the strap and vary it as λ^3.

TABLE II.- PERTINENT PARAMETERS OF SPACECRAFT

Parameter	1/11-scale model		Full scale	
Tricycle landing-gear configurations:				
Mass	0.337 slug	4.92 kg	449 slug	6 550 kg
Moment of inertia:				
I_{XX} (roll)	0.0319 slug-ft^2	0.0432 kg-m^2	5 140 slug-ft^2	6 970 kg-m^2
I_{YY} (pitch)	0.1854 slug-ft^2	0.2514 kg-m^2	29 860 slug-ft^2	40 480 kg-m^2
I_{ZZ} (yaw)	0.1966 slug-ft^2	0.2666 kg-m^2	31 660 slug-ft^2	42 930 kg-m^2
Body:				
Length	2.54 ft	0.774 m	27.94 ft	8.516 m
Planform area	2.32 ft^2	0.215 m^2	280.7 ft^2	26.08 m^2
Basic configuration:				
Mass	0.326 slug	4.76 kg	434 slug	6 330 kg
Moment of inertia:				
I_{XX} (roll)	0.0318 slug-ft^2	0.0431 kg-m^2	5 120 slug-ft^2	6 940 kg-m^2
I_{YY} (pitch)	0.1662 slug-ft^2	0.2253 kg-m^2	26 770 slug-ft^2	36 300 kg-m^2
I_{ZZ} (yaw)	0.1830 slug-ft^2	0.2481 kg-m^2	29 470 slug-ft^2	39 960 kg-m^2
Body:				
Length	2.54 ft	0.774 m	27.94 ft	8.516 m
Planform area	2.32 ft^2	0.215 m^2	280.7 ft^2	26.08 m^2

TABLE III.- ACCELEROMETER CHARACTERISTICS

Accelerometer orientation	Range, g units	Natural frequency, cps (Hz)	Damping, percent of critical damping	Limiting flat frequency of other recording equipment, cps (Hz)
Tricycle landing-gear configurations:				
Normal (at vehicle center of gravity)	±15	183	60	120
Longitudinal (at vehicle center of gravity)	±15	154	65	120
Basic configurations:				
Normal (at vehicle center of gravity)	±50	633	70	120
Longitudinal (at vehicle center of gravity)	±25	360	65	120

TABLE IV.- SUMMARY OF RESULTS OF RUNWAY LANDINGS USING TRICYCLE LANDING-GEAR CONFIGURATIONS

[All values are full scale unless otherwise indicated. L denotes left displacement; R denotes right displacement.]

Vertical velocity		Horizontal velocity		Pitch, deg	Roll, deg	Yaw, deg	Torque		Nose gear strain strap composition (model scale)			Nose gear stroke		Rear gear strain strap composition (model scale)			Rear gear stroke				Length of slideout from launch		Lateral displacement		Stability
									No. of wires	Diameter of wires				No. of wires	Diameter of wires		Right		Left					
ft/sec	m/s	ft/sec	m/s				ft-lb	m-N		in.	mm	in.	cm		in.	mm	in.	cm	in.	cm	ft	m	ft	m	
Tricycle gear with free swivel nose wheel																									
10	3.0	206	62.8	25	0	0	None	None	1	0.03	0.76	7.6	19	2	0.03	0.76	6.2	16	8.6	22	1580	482	L 11	L 3.4	
10	3.0	209	63.7	25	0	0	None	None	1	.03	.76	6.8	17	2	.03	.76	7.9	20	8.4	21	1590	485	L 11	L 3.4	
10	3.0	209	63.7	25	0	0	None	None	1	.03	.76	8.2	21	2	.03	.76	8.9	23	6.8	17	1700	518	R 5	R 2	
10	3.0	209	63.7	25	0	0	None	None	1	.03	.76	5.7	14	2	.03	.76	8.9	23	7.6	19	1690	515	R 9	R 3	
10	3.0	212	64.6	25	0	0	None	None	1	.03	.76	7.3	19	2	.03	.76	7.7	20	7.7	20	1720	524	0	0	
10	3.0	212	64.6	25	0	0	None	None	1	.03	.76	5.9	15	2	.03	.76	6.9	18	8.9	23	1720	524	0	0	
10	3.0	209	63.7	25	0	0	None	None	1	.03	.76	6.8	17	2	.03	.76	7.7	20	6.9	18	1760	536	R 66*	R 20*	
10	3.0	206	62.8	25	0	0	None	None	1	.03	.76	10.5**	27**	2	.03	.76	6.6	17	8.1	21	1670	509	R 33	R 10	
10	3.0	206	62.8	25	0	0	None	None	1	.03	.76	8.1	21	2	.03	.76	7.6	19	7.7	20	1770	539	0	0	
10	3.0	209	63.7	25	0	L 10	None	None	1	.03	.76	10.5**	27**	2	.03	.76	6.0	15	9.4	24	1450	442	L 55	L 17	
10	3.0	209	63.7	25	0	L 10	None	None	1	.03	.76	10.5**	27**	2	.03	.76	6.3	16	8.8	22	1510	460	R 66*	R 20*	
10	3.0	206	62.8	25	0	L 10	None	None	1	.03	.76	10.5**	27**	2	.03	.76	8.8	22	6.6	17	1440	439	R 55	R 17	
10	3.0	209	63.7	25	0	L 10	None	None	1	.03	.76	10.5**	27**	2	.03	.76	6.6	17	8.8	22	1460	445	L 44	L 13	
Tricycle gear with torque-steering nose wheel																									
10	3.0	219	66.8	25	0	0	L 312	L 423	2	0.02	0.51	10.5**	27**	2	0.03	0.76	8.1	21	8.8	22	1810	552	L 121*	L 37*	
10	3.0	212	64.6	25	0	0	L 312	L 423	1	.03	.76	9.2	23	2	.03	.76	7.0	18	6.2	16	1650	503	L 77	L 23	
10	3.0	222	67.7	25	0	0	L 312	L 423	1	.03	.76			2	.03	.76					1760	536	L 121*	L 37*	
10	3.0	219	66.8	25	0	0	L 312	L 423	1	.03	.76	10.5**	27**	2	.03	.76	7.6	19	6.7	17	1760	536	L 88	L 27	
10	3.0	209	63.7	25	0	0	L 312	L 423	1	.03	.76	10.5**	27**	2	.03	.76	7.3	19	6.7	17	1720	524	L 121*	L 37*	
10	3.0	199	60.7	25	0	0	L 312	L 423	1	.03	.76	5.9	15	2	.03	.76	6.2	16	6.7	17	1530	466	L 55	L 17	
10	3.0	202	61.6	25	0	0	L 918	L 1240	1	.03	.76	9.9	25	2	.03	.76	7.8	20	6.2	16	1580	482	L 88	L 27	
10	3.0	212	64.6	25	0	0	L 918	L 1240	1	.03	.76	9.7	25	2	.03	.76	9.7	25	6.8	17	1650	503	L 121*	L 37*	
10	3.0	219	66.8	25	0	0	R 312	R 423	2	.02	.51	10.5**	27**	2	.03	.76	5.7	14	8.1	21	1750	533	R 22	R 7	
10	3.0	212	64.6	25	0	0	R 312	R 423	2	.02	.51	10.5**	27**	2	.03	.76	8.2	21	8.2	21	1580	482	R 66*	R 20*	
10	3.0	206	62.8	25	0	0	R 312	R 423	2	.03	.76	8.1	21	2	.03	.76	7.7	20	8.8	22	1590	485	R 55	R 17	
10	3.0	212	64.6	25	0	0	R 312	R 423	2	.03	.76	10.1	26	2	.03	.76	7.3	19	7.9	20	1670	509	R 66*	R 20*	
10	3.0	202	61.6	25	0	L 10	L 360	L 488	2	.03	.76	10.5**	27**	2	.03	.76	**	**	5.5	14	1140	347	R 66*	R 20*	Turnover
10	3.0	219	66.8	25	0	L 10	L 360	L 488	2	.03	.76	10.5**	27**	2	.03	.76	8.5	22	9.4	24	1620	494	L 121*	L 37*	
10	3.0	206	62.8	25	0	L 10	L 360	L 488	2	.03	.76	10.5**	27**	3	.02	.51	**	**	8.2	21	1500	457	R 44	R 13	
10	3.0	202	61.6	25	0	L 10	L 360	L 488	2	.03	.76	8.8	22	3	.02	.51	11.0	28	**	**	1470	448	L 121*	L 37*	
10	3.0	209	63.7	25	0	L 10	L 722	L 979	2	.03	.76	9.2	23	3	.02	.51	**	**	**	**	1530	466	L 121*	L 37*	
10	3.0	202	61.6	25	0	L 10	L 722	L 979	2	.03	.76	9.7	25	3	.02	.51	12.6	32	11.6	29	1600	488	L 66	L 20	
10	3.0	199	60.7	25	0	L 10	L 722	L 979	2	.03	.76	10.5**	27**	3	.02	.51	11.0	28	**	**	1500	457	L 121*	L 37*	

*Model hit restraining screen.

**Strut bottomed.

TABLE V.- SUMMARY OF RESULTS OF RUNWAY SLIDEOUT TEST USING TRICYCLE LANDING-GEAR CONFIGURATIONS

[All values are full scale unless otherwise indicated. L denotes left displacement; R denotes right displacement. Rear gear or nose gear stroke is either small or no stroke (not recorded).]

Vertical velocity		Horizontal velocity		Pitch, deg	Roll, deg	Yaw, deg	Torque		Nose gear strain strap composition (model scale)			Rear gear strain strap composition (model scale)			Length of slideout from launch		Lateral displacement		Stability
									No. of wires	Diameter of wires		No. of wires	Diameter of wires						
ft/sec	m/s	ft/sec	m/s				ft-lb	m-N		in.	mm		in.	mm	ft	m	ft	m	
Tricycle gear with free-swivel nose wheel																			
2	0.6	199	60.7	0	0	0	None	None	2	0.04	1.02	2	0.04	1.02	1460	445	None	None	
2	.6	199	60.7	0	0	0	None	None	2	.01	.25	2	.04	1.02	1460	445	L 33	L 10	
									1	.02	.51	2	.04	1.02					
2	.6	199	60.7	0	0	0	None	None	1	.01	.25	2	.04	1.02	1460	445	L 33	L 10	
									1	.02	.51	2	.04	1.02					
2	.6	202	61.6	0	0	0	None	None	1	.01	.25	2	.04	1.02	1420	433	L 22	L 7	
Tricycle gear with torque-steering nose wheel																			
2	0.6	202	61.6	0	0	0	L 514	L 697	1	0.02	0.51	2	0.04	1.02	1430	436	L 121*	L 37*	
2	.6	192	58.5	0	0	0	L 514	L 697	1	.02	.51	2	.04	1.02	1400	427	L 121*	L 37*	
2	.6	189	57.6	0	0	0	L 1029	L 1395	1	.02	.51	2	.04	1.02	1320	402	L 121*	L 37*	
2	.6	206	62.8	0	0	0	L 1029	L 1395	1	.02	.51	2	.04	1.02	1390	424	L 28	L 9	Turnover
Tricycle gear with roll steering (camber)																			
2	0.6	199	60.7	0	L 5	0	None	None	2	0.04	1.02	2	0.04	1.02	1480	451	L 121*	L 37*	
2	.6	196	59.7	0	L 10	0	None	None	2	.04	1.02	2	.04	1.02	1210	369	L 121*	L 37*	Turnover
2	.6	206	62.8	0	R 5	0	None	None	1	.02	.51	2	.04	1.02	1200	366	R 66*	R 20*	
Tricycle gear with torque-steering nose wheel and roll steering (camber)																			
2	0.6	206	62.8	0	R 5	0	L 514	L 697	1	0.02	0.51	2	0.04	1.02	1520	463	R 33	R 10	
2	.6	209	63.7	0	R 5	0	L 514	L 697	1	.02	.51	2	.04	1.02	1540	469	R 11	R 3	
Tricycle gear with nose skid																			
2	0.6	199	60.7	0	0	0	None	None	2	0.04	1.02	2	0.04	1.02	1180	360	None	None	
2	.6	196	59.7	0	0	0	None	None	2	.04	1.02	2	.04	1.02	1140	347	L 11	L 3	
2	.6	196	59.7	0	L 5	0	None	None	2	.04	1.02	2	.04	1.02	1190	363	None	None	
2	.6	196	59.7	0	L 5	0	None	None	2	.04	1.02	2	.04	1.02	1140	347	None	None	
2	.6	196	59.7	0	L 7.5	0	None	None	2	.04	1.02	2	.04	1.02	1200	336	None	None	
2	.6	196	59.7	0	L 7.5	0	None	None	2	.04	1.02	2	.04	1.02	1200	336	None	None	
2	.6	192	58.5	0	L 10	0	None	None	2	.04	1.02	2	.04	1.02	1210	369	------	-----	Turnover
2	.6	196	59.7	0	L 10	0	None	None	2	.04	1.02	2	.04	1.02	1030	314	L 66	L 20	Turnover
2	.6	199	60.7	0	L 10	0	None	None	2	.04	1.02	2	.04	1.02	1140	347	------	-----	Turnover

*Model hit restraining screen.

TABLE VI.- RUNWAY LANDINGS USING FREE-SWIVELING NOSE-WHEEL CONFIGURATION

[All values are full scale; all runs were stable]

Vertical velocity		Horizontal velocity		Landing attitude, deg	Maximum normal acceleration, g units	Maximum longitudinal acceleration, g units
ft/sec	m/s	ft/sec	m/s			
10	3.0	213	64.9	25	4.9	1.4
10	3.0	213	64.9	25	5.6	1.2
10	3.0	209	63.7	25	5.5	1.4
10	3.0	205	62.5	25	5.3	1.1
10	3.0	207	63.1	25	4.6	1.3

TABLE VII.- RUNWAY LANDINGS USING BASIC CONFIGURATION

[All values are full scale]

Vertical velocity		Horizontal velocity		Landing attitude, deg	Maximum normal acceleration, g units	Maximum longitudinal acceleration, g units	Remarks
ft/sec	m/s	ft/sec	m/s				
10	3.0	332	101.0	15	9.2	4.9	No touchdown shock
10	3.0	332	101.0	15	17.4	3.8	absorbing tab
10	3.0	332	101.0	15	12.0	2.5	
10	3.0	332	101.0	15	30.1	5.4	
10	3.0	345	105.0	15	21.4	---	
10	3.0	342	104.0	15	16.6	2.2	Using touchdown
10	3.0	342	104.0	15	18.7	4.0	shock absorbing
10	3.0	342	104.0	15	23.6	5.0	tab
10	3.0	352	107.0	15	30.7	---	
10	3.0	335	102.0	15	8.6	2.6	
10	3.0	325	99.1	15	9.5	4.4	
10	3.0	325	99.1	15	17.4	5.4	
10	3.0	266	81.1	20	7.2	3.1	
10	3.0	249	75.9	20	12.2	3.3	
10	3.0	249	75.9	20	7.6	3.5	
10	3.0	216	65.8	30	18.7	4.2	
10	3.0	216	65.8	30	13.2	4.4	
10	3.0	216	65.8	30	21.5	6.8	

TABLE VIII.- HORIZONTAL-TYPE CALM-WATER LANDINGS

[All values are full scale]

Vertical velocity		Horizontal velocity		Landing attitude, deg	Normal acceleration, g units			Longitudinal acceleration, g units		
ft/sec	m/s	ft/sec	m/s		1st impact	2d impact	3d impact (*)	1st impact	2d impact	3d impact
1.5	0.46	262	79.8	25	7.0	6.4	-10.3	0.6	1.7	5.3
1.5	.46	249	75.9	25	6.1	5.4	-2.6	.7	4.8	1.5
1.5	.46	259	78.9	25	6.3	4.4	-4.6	.8	3.2	3.1

*Model came to rest in an inverted position as indicated by the negative normal acceleration in the third impact.

TABLE IX.- VERTICAL PARACHUTE-TYPE CALM-WATER LANDINGS

[All values are full scale]

Vertical velocity		Horizontal velocity		Landing attitude, deg	Normal acceleration, g units		Longitudinal acceleration, g units		Stability
ft/sec	m/s	ft/sec	m/s		1st impact	2d impact	Spike	Sustained	
40	12	0	0	100	-0.8	-8.2	-8.3	-2.6	Vehicle comes to rest inverted
40	12	0	0	95	-.4	---	-6.4	-2.8	Vehicle comes to rest inverted
40	12	0	0	90	.5	5.6	-5.5	-2.6	Vehicle comes to rest right side up
40	12	0	0	90	.5	5.0	-3.8	-2.6	Vehicle comes to rest right side up
40	12	0	0	85	1.1	---	-7.3	-2.4	Vehicle comes to rest right side up
40	12	0	0	80	1.9	---	-6.9	-2.0	Vehicle comes to rest right side up
40	12	0	0	-70	3.0	---	----	2.2	Vehicle comes to rest right side up
40	12	0	0	-75	2.7	---	----	2.5	Vehicle comes to rest right side up
40	12	0	0	-80	2.3	2.8	----	2.9	Vehicle comes to rest right side up
40	12	0	0	-85	1.4	7.1	----	3.2	Vehicle comes to rest right side up
40	12	0	0	-90	.5	-6.6	----	3.8	Vehicle comes to rest inverted
40	12	0	0	-90	.3	---	----	3.9	Vehicle comes to rest inverted
50	15	0	0	85	1.8	---	-8.1	-2.6	Vehicle comes to rest right side up
50	15	0	0	-85	1.6	3.2	----	3.7	Vehicle comes to rest right side up
60	18	0	0	85	1.4	---	-10.5	-2.6	Vehicle comes to rest right side up
60	18	0	0	-85	1.9	3.8	----	3.9	Vehicle comes to rest right side up

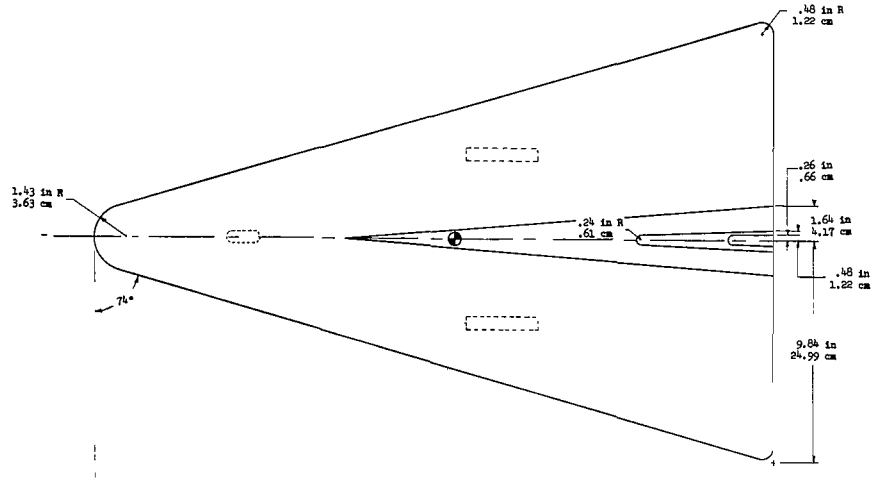

Ordinates for body shapes

x		+ y		− y	
in	cm	in	cm	in	cm
0	0	0	0	0	0
3.82	9.70	2.27	5.77	2.73	6.93
7.64	19.41	2.51	6.38	3.65	9.27
11.45	29.08	2.51	6.38	4.04	10.26
15.27	38.79	2.41	6.12	3.91	9.93
19.09	48.49	2.23	5.66	3.27	8.31
22.90	58.17	1.92	4.88	2.41	6.12
26.72	67.87	1.54	3.91	1.40	3.56
30.54	77.57	1.05	2.67	.37	.94

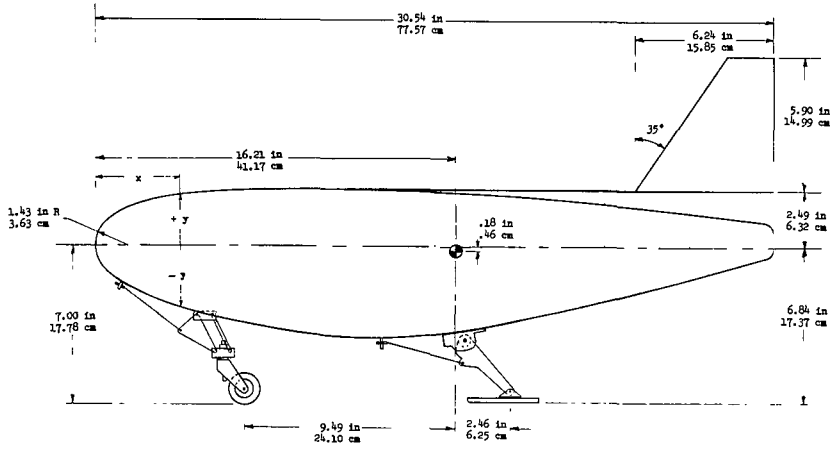

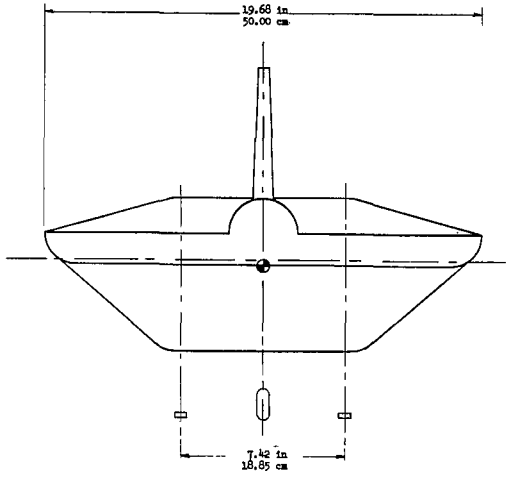

Figure 1.- General arrangement of 1/11-scale HL-10 model with tricycle landing gear. (All dimensions are model scale.)

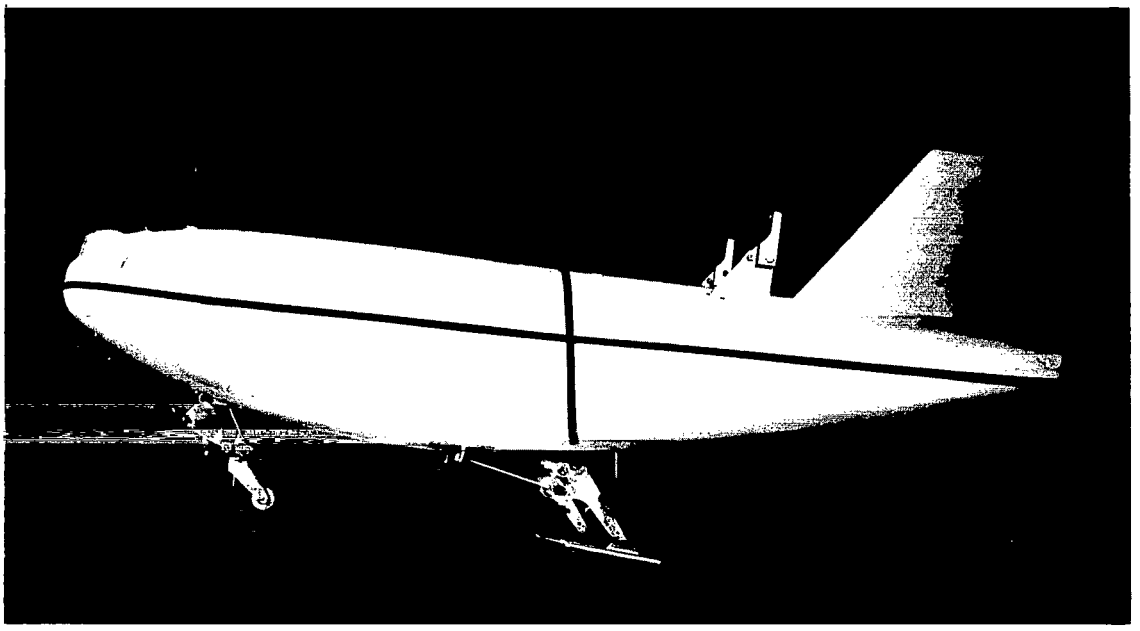

(a) Side view. L-63-9642

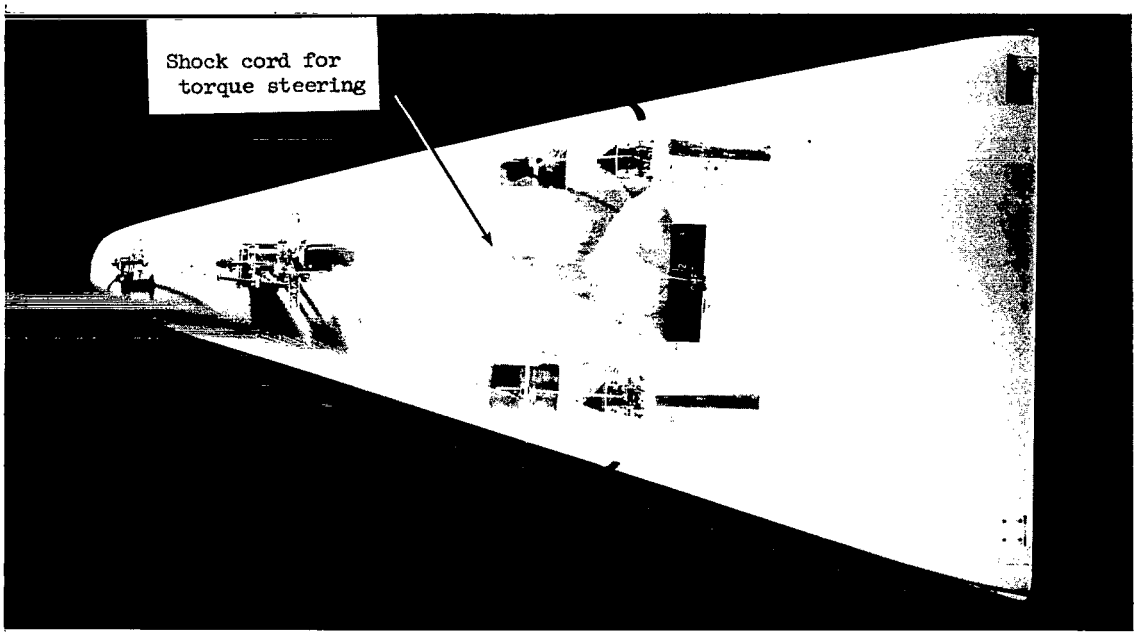

(b) Bottom view. L-63-9641

Figure 2.- Photographs of model showing tricycle landing gear.

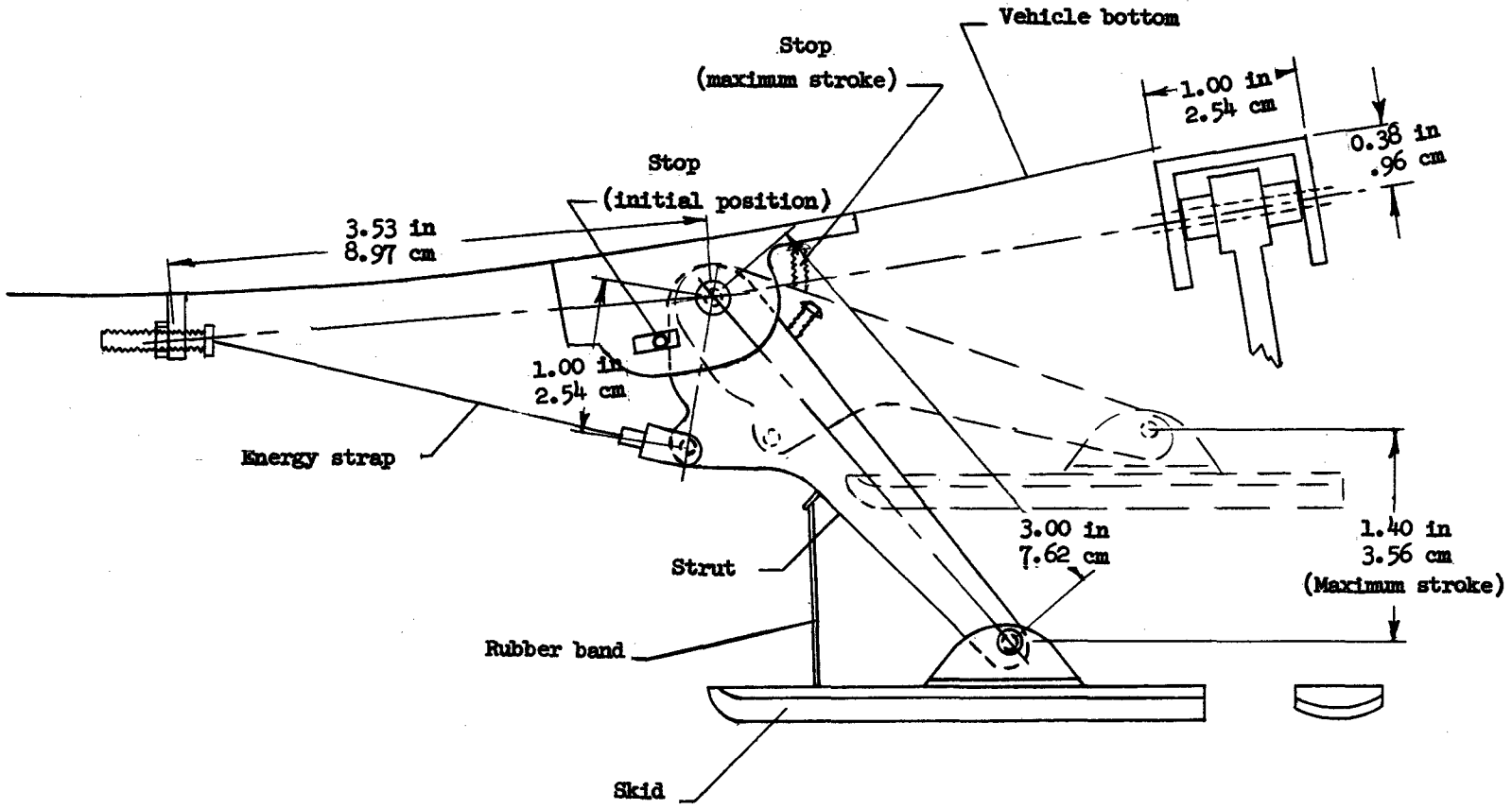

(a) Rear main gear.

Figure 3.- Details of tricycle landing-gear assemblies. (All dimensions are model scale.)

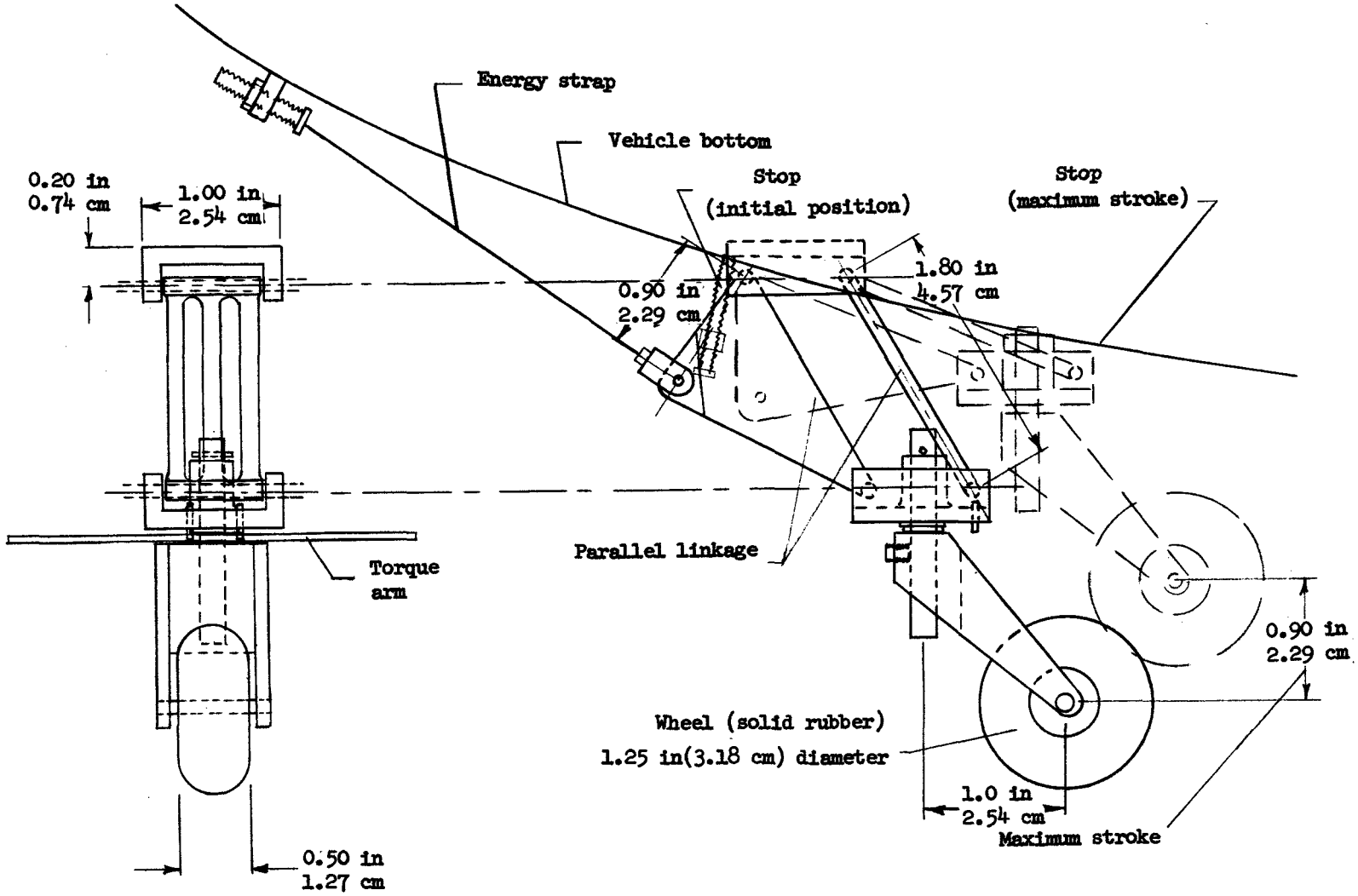

(b) Nose-wheel arrangement.

Figure 3.- Continued.

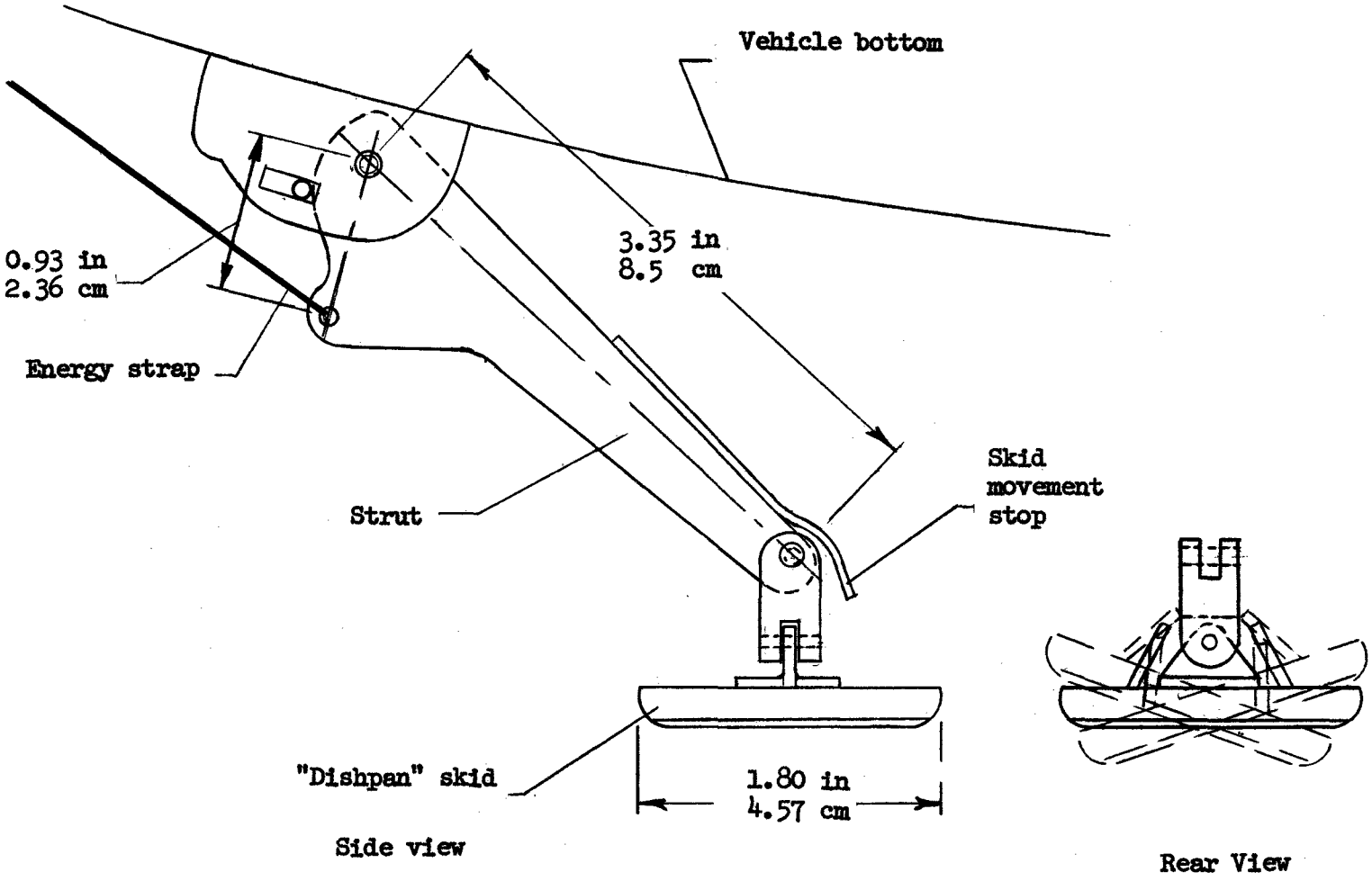

(c) Nose-skid arrangement.

Figure 3.- Concluded.

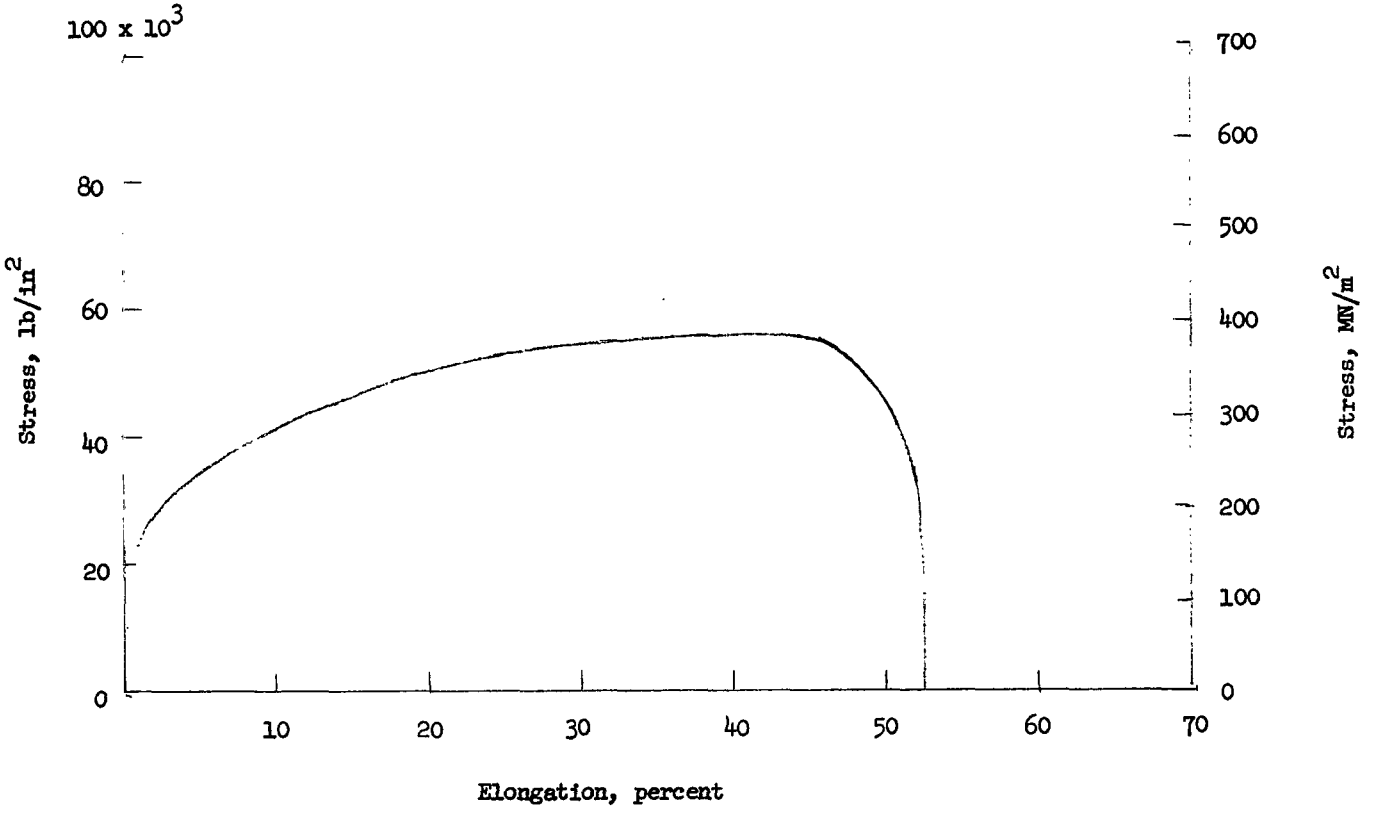

Figure 4.- Stress strain characteristics of low-carbon nickel wire used as an energy strap for landing impact attenuation on the tricycle landing-gear configuration.

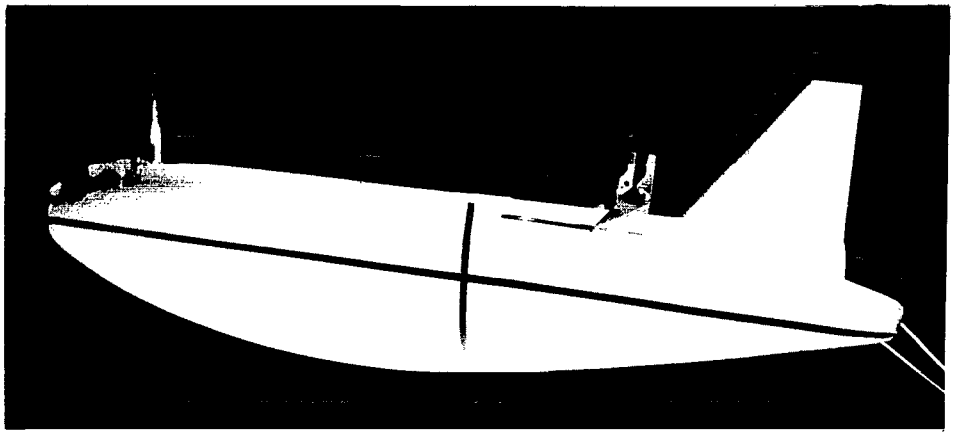

(a) Basic configuration. L-63-6015

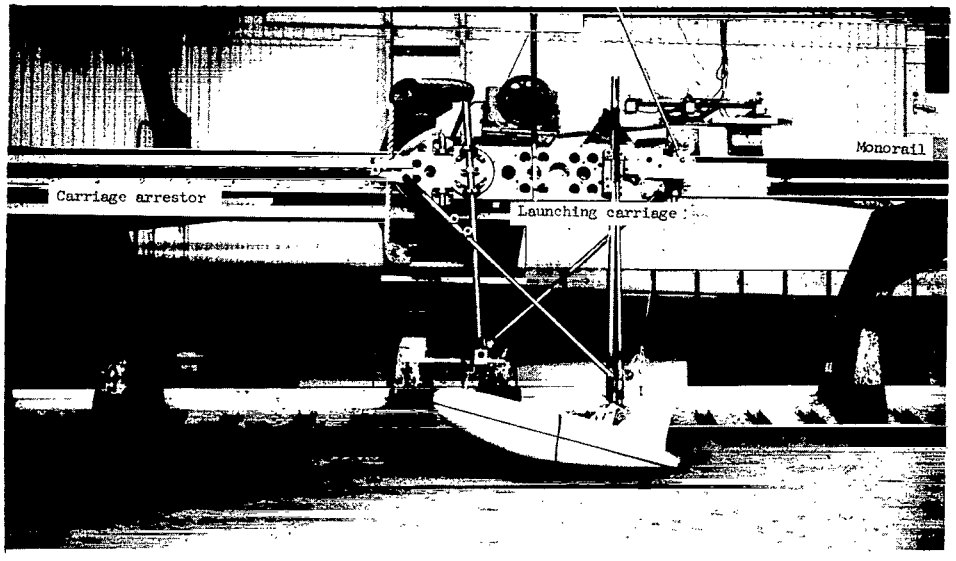

(b) Model on launch apparatus. L-63-6012

(c) Model with braking parachute. L-63-6195

Figure 5.- Photographs of skid-rocker configuration.

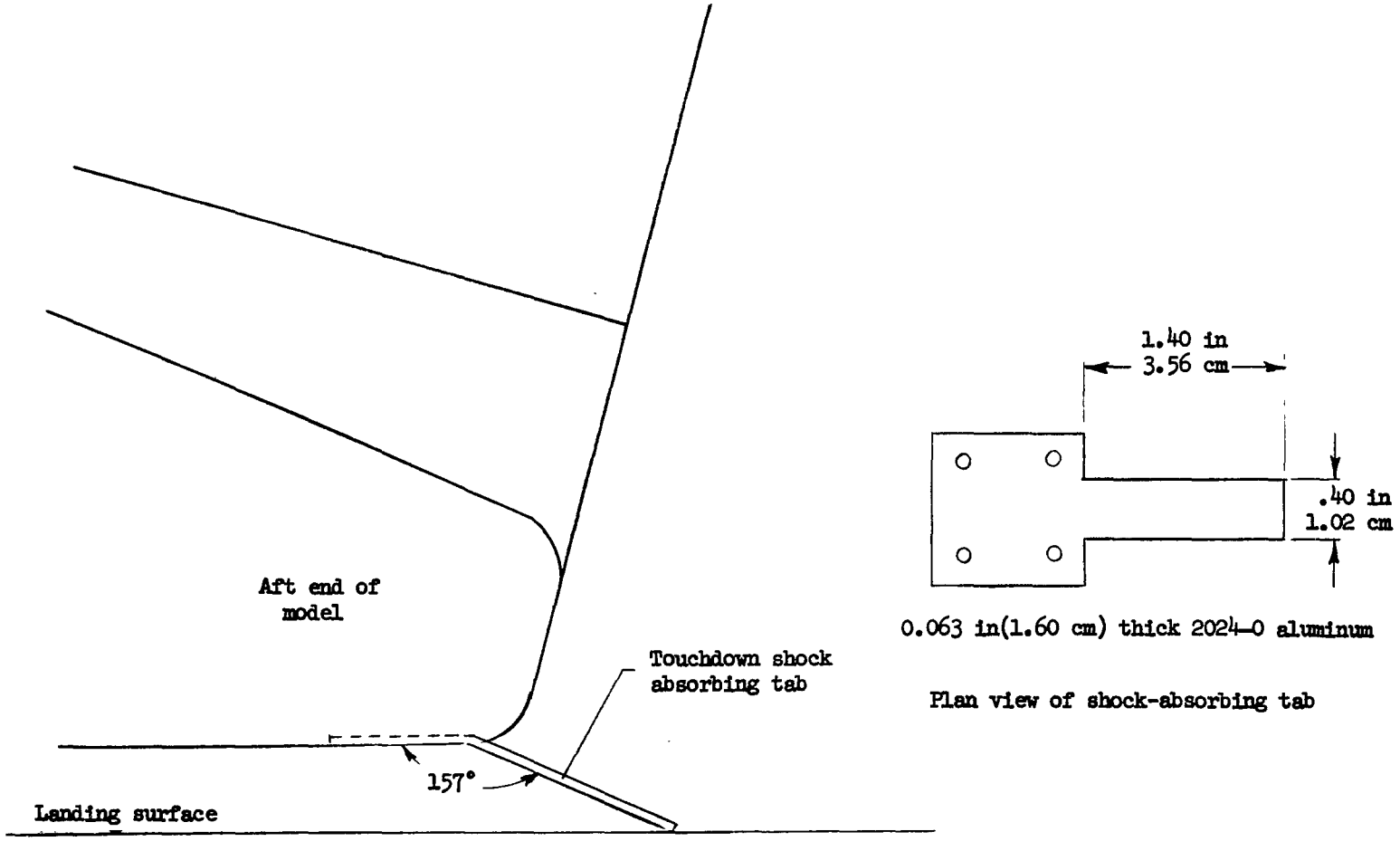

Figure 6.- Sketch of shock-absorbing tab used on skid-rocker configuration for runway landings.

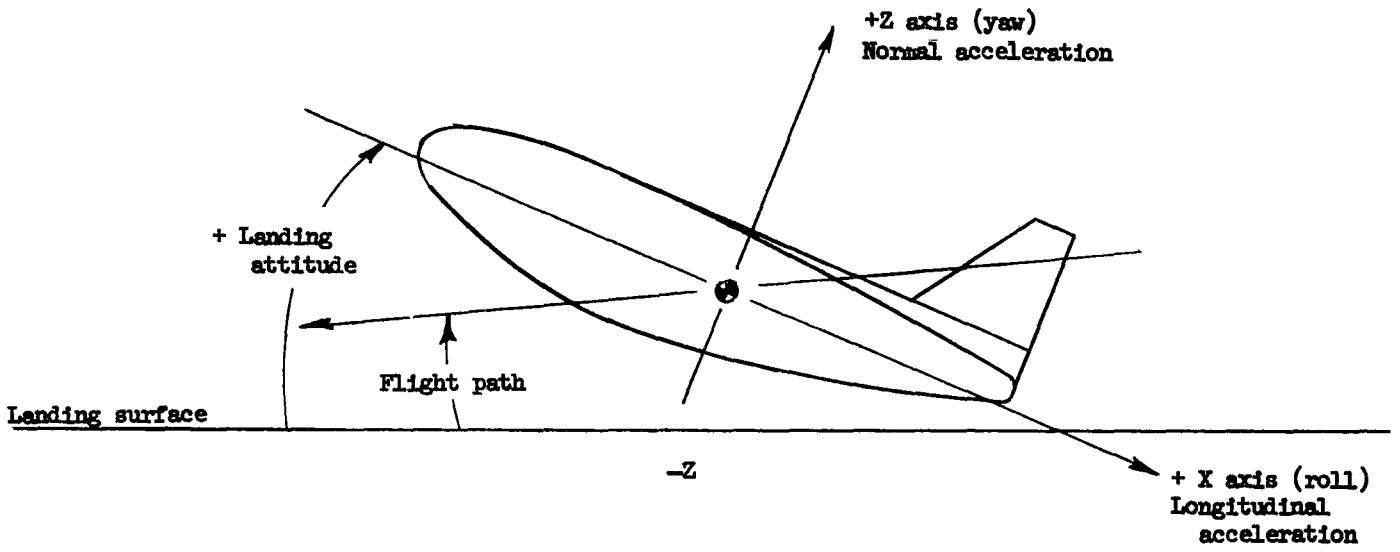

Figure 7.- Sketch identifying acceleration axes, landing attitude, and flight path.

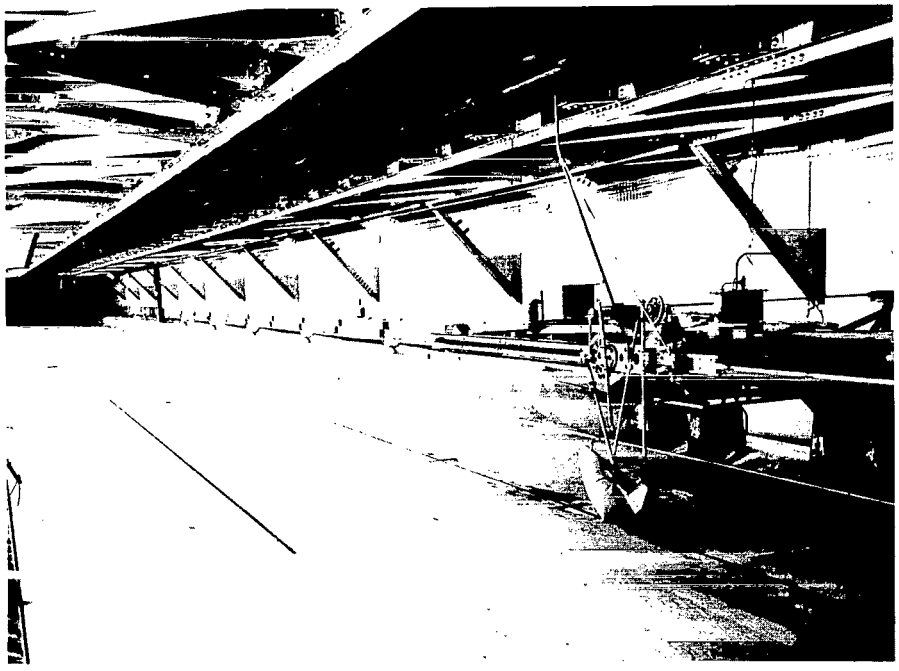

(a) Plywood runway. L-63-9325

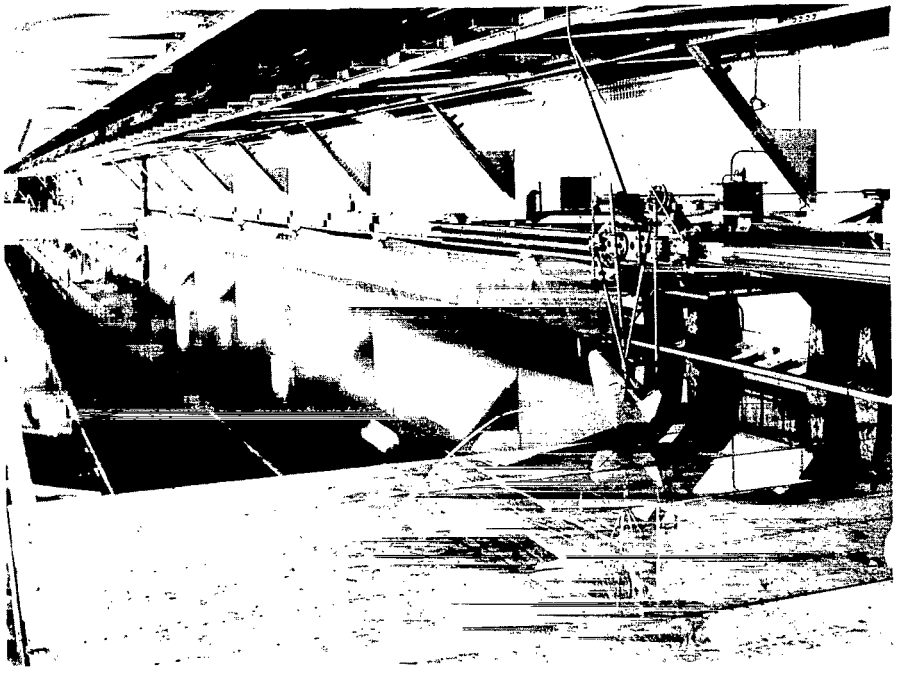

(b) Calm water. L-64-1279

Figure 8.- Photographs of horizontal landing apparatus used for hard-surface and water landing tests.

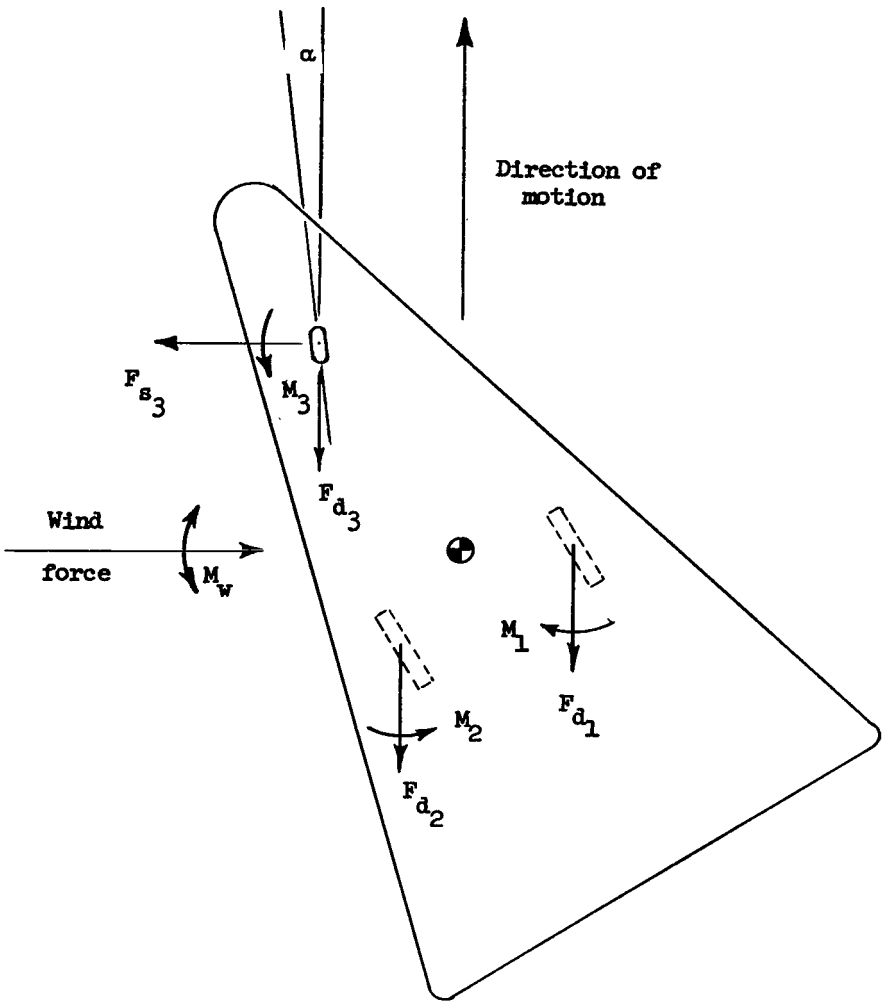

α	Angle wheel makes with direction of motion
F_{d_1}	Drag force of right rear skid
F_{d_2}	Drag force of left rear skid
F_{d_3}	Drag force of nose wheel
F_{s_3}	Side force of nose wheel
M_1	Moment produced by right rear skid
M_2	Moment produced by left rear skid
M_3	Moment produced by nose wheel
M_w	Moment produced by wind force

Figure 9.- Sketch showing forces and moments on vehicle in a left roll slideout condition.

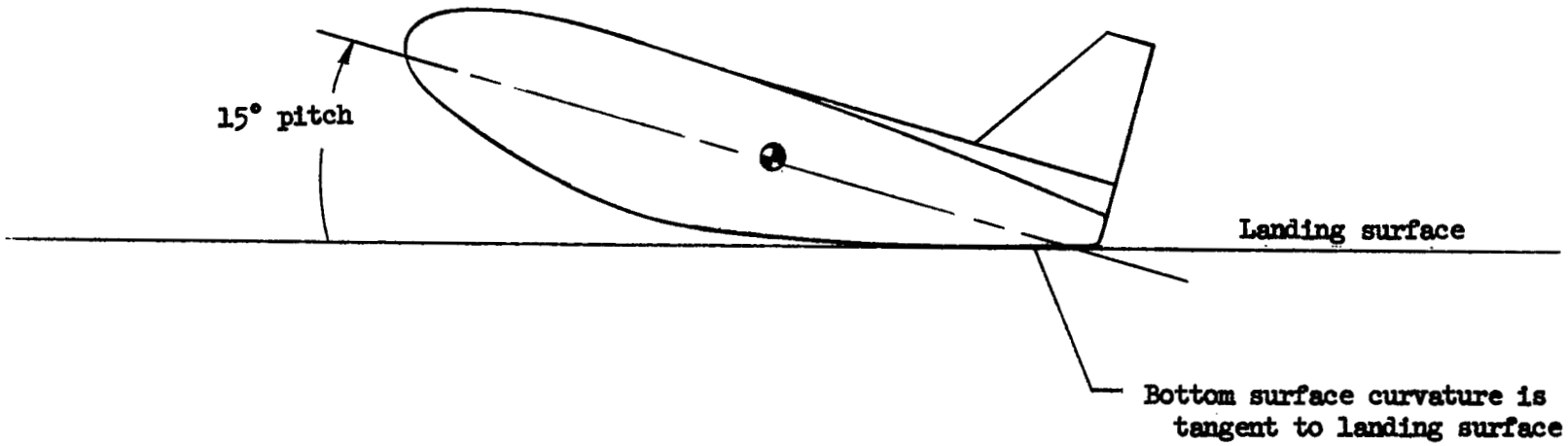

Figure 10.- Sketch showing 15° landing attitude at which aft undersurface curvature is tangent to landing surface.

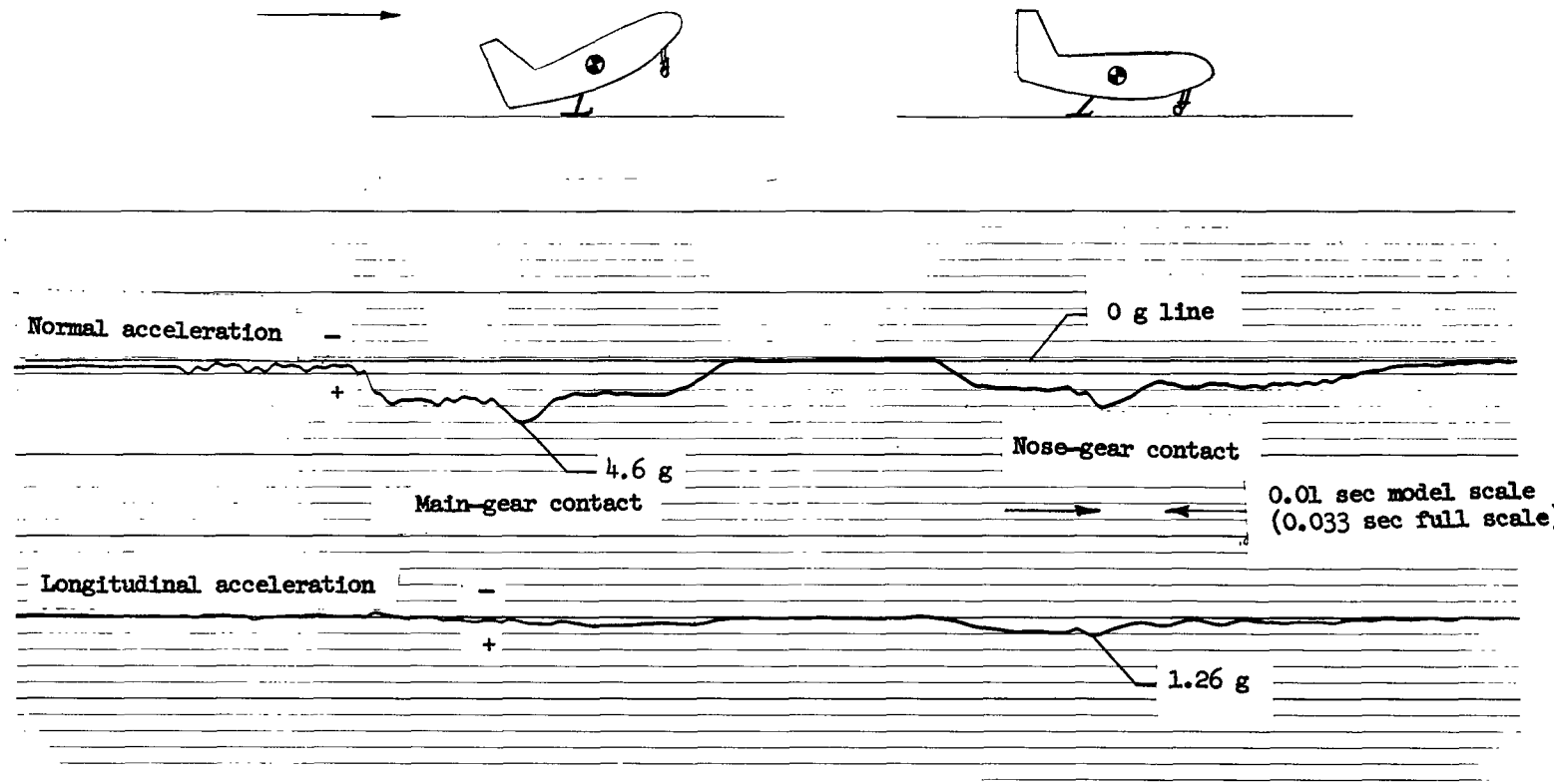

Figure 11.- Typical oscillograph records of accelerations using the tricycle landing gear with free-swiveling nose wheel. Vertical velocity, 10 ft/sec (3.0 m/s); horizontal velocity, 207 ft/sec (63.1 m/s); landing attitude, 25°. (All values are full scale unless otherwise indicated.)

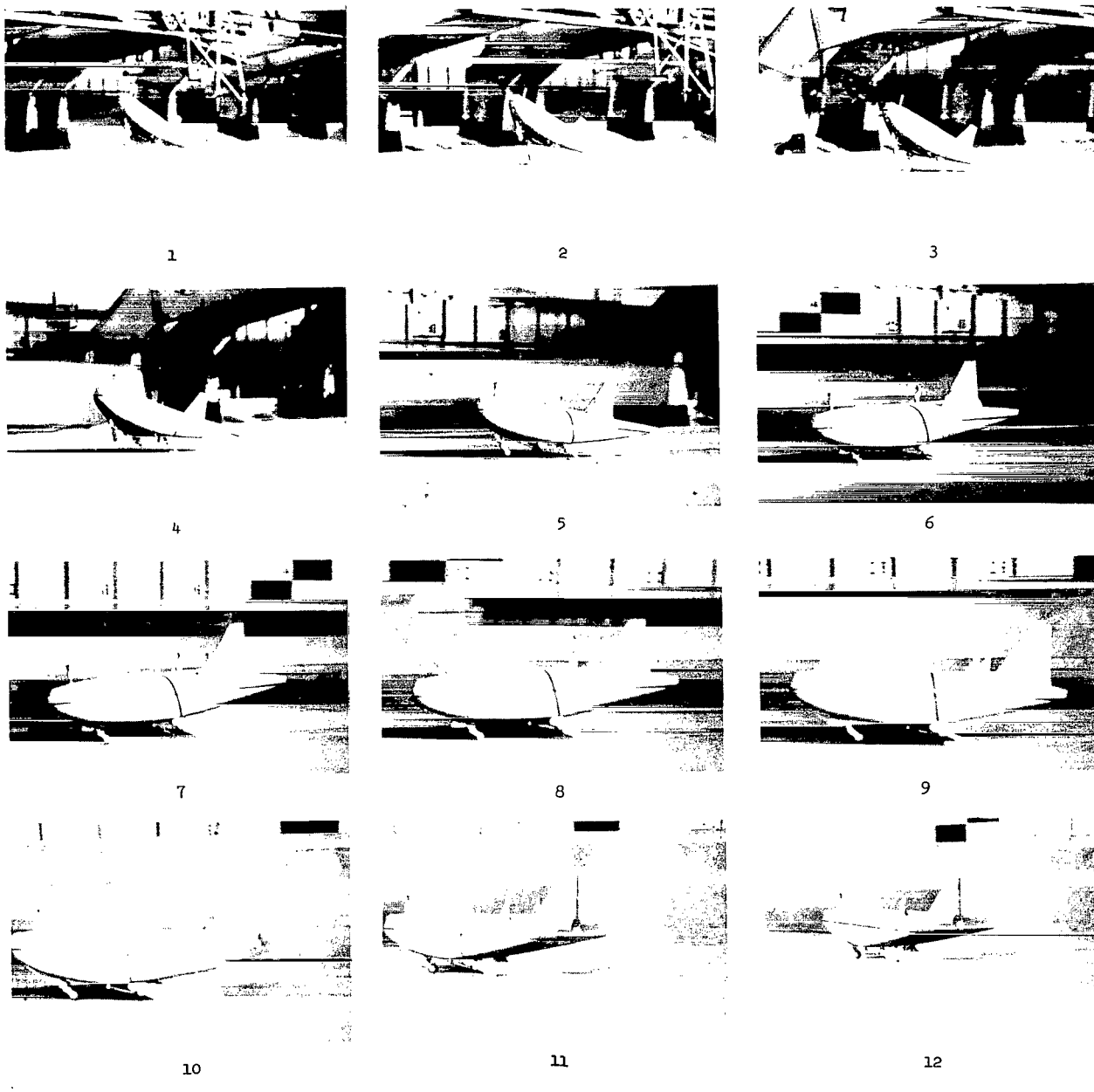

L-66-4539

Figure 12.- Typical sequence photographs of a landing using the tricycle landing gear with a free-swiveling nose wheel. Vertical velocity, 10 ft/sec (3.0 m/s); horizontal velocity, 209 ft/sec (63.7 m/s); landing attitude, 25^{0}. (All values are full scale.)

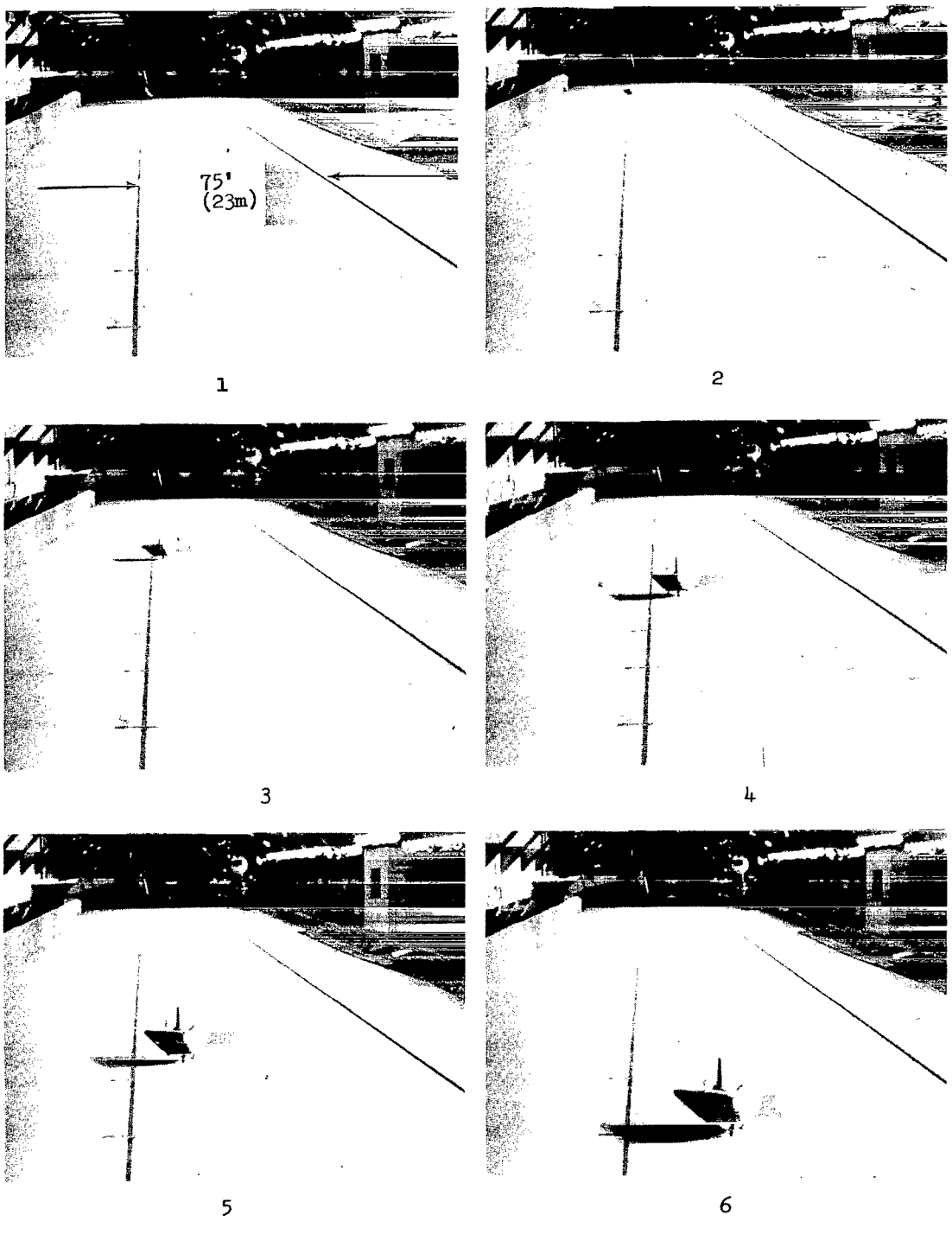

(a) 0^0 roll.

L-66-4540

Figure 13.- Typical sequence photographs of slideout tests using the tricycle landing gear with a free-swiveling nose wheel and roll steering. Vertical velocity, 2 ft/sec (0.6 m/s); horizontal velocity approximately 200 ft/sec (61 m/s); attitude, 0^0. (All values are full scale.)

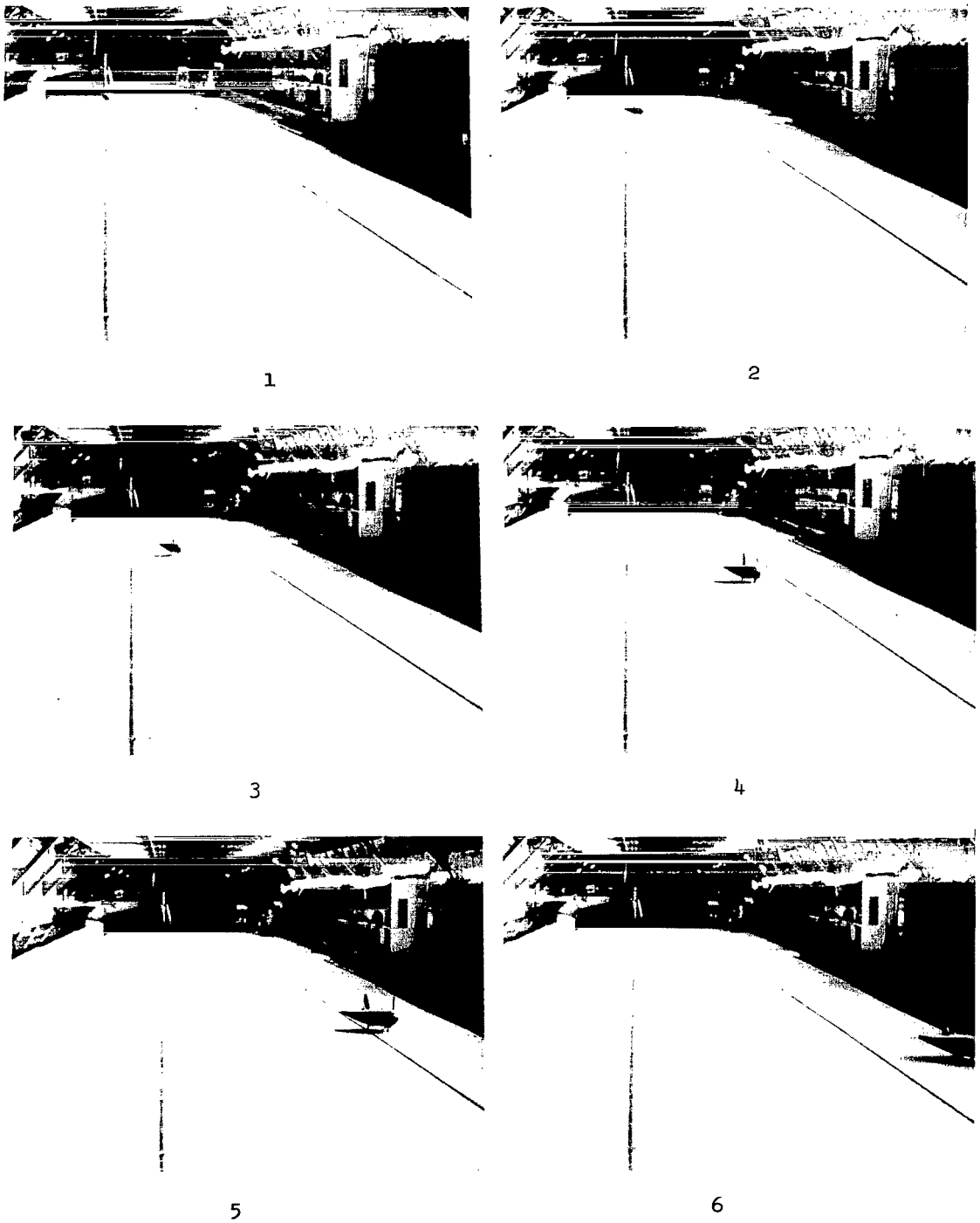

(b) 5^{0} left roll. L-66-4541

Figure 13.- Continued.

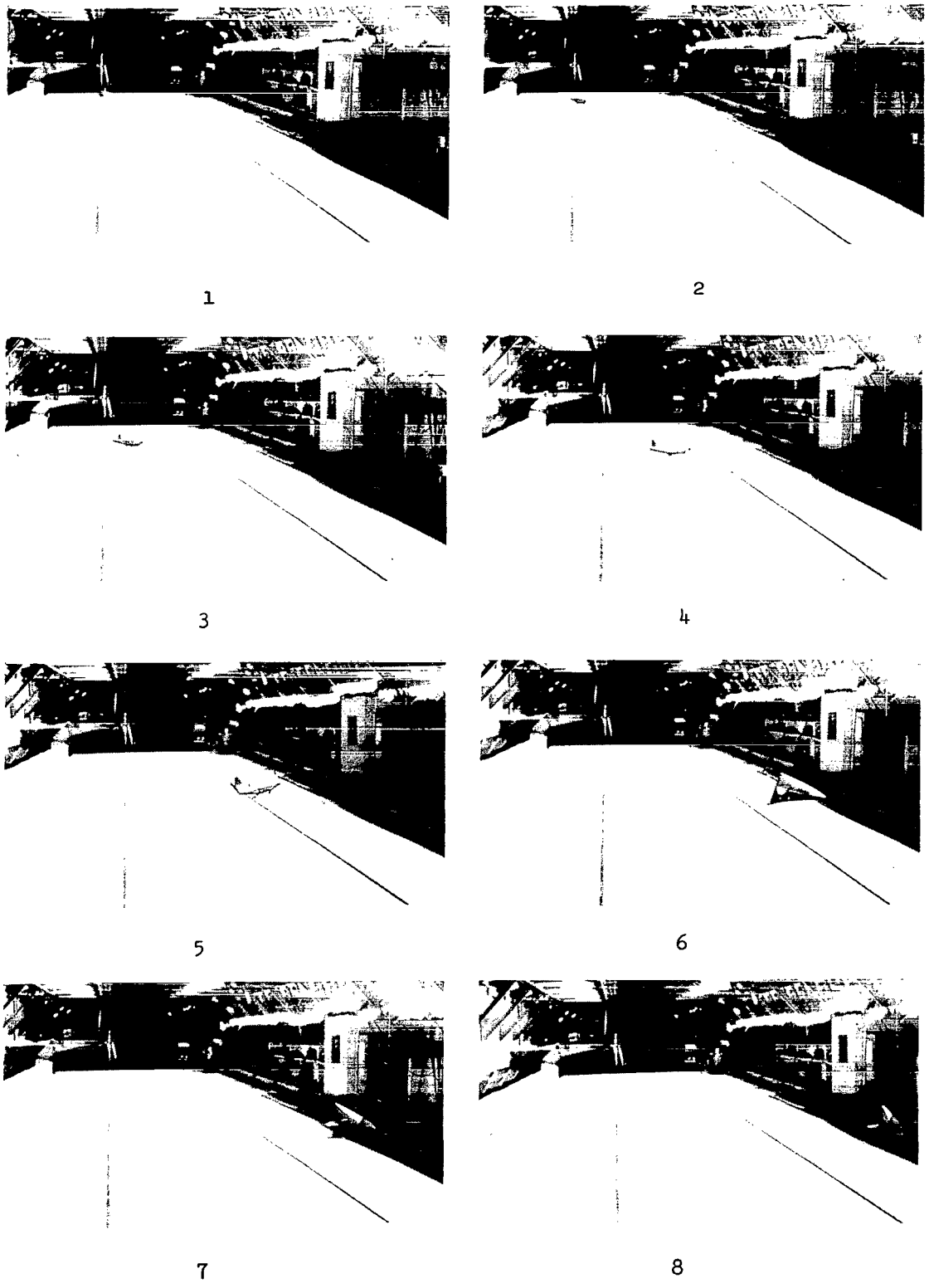

(c) 10^0 left roll. L-66-4542

Figure 13.- Concluded.

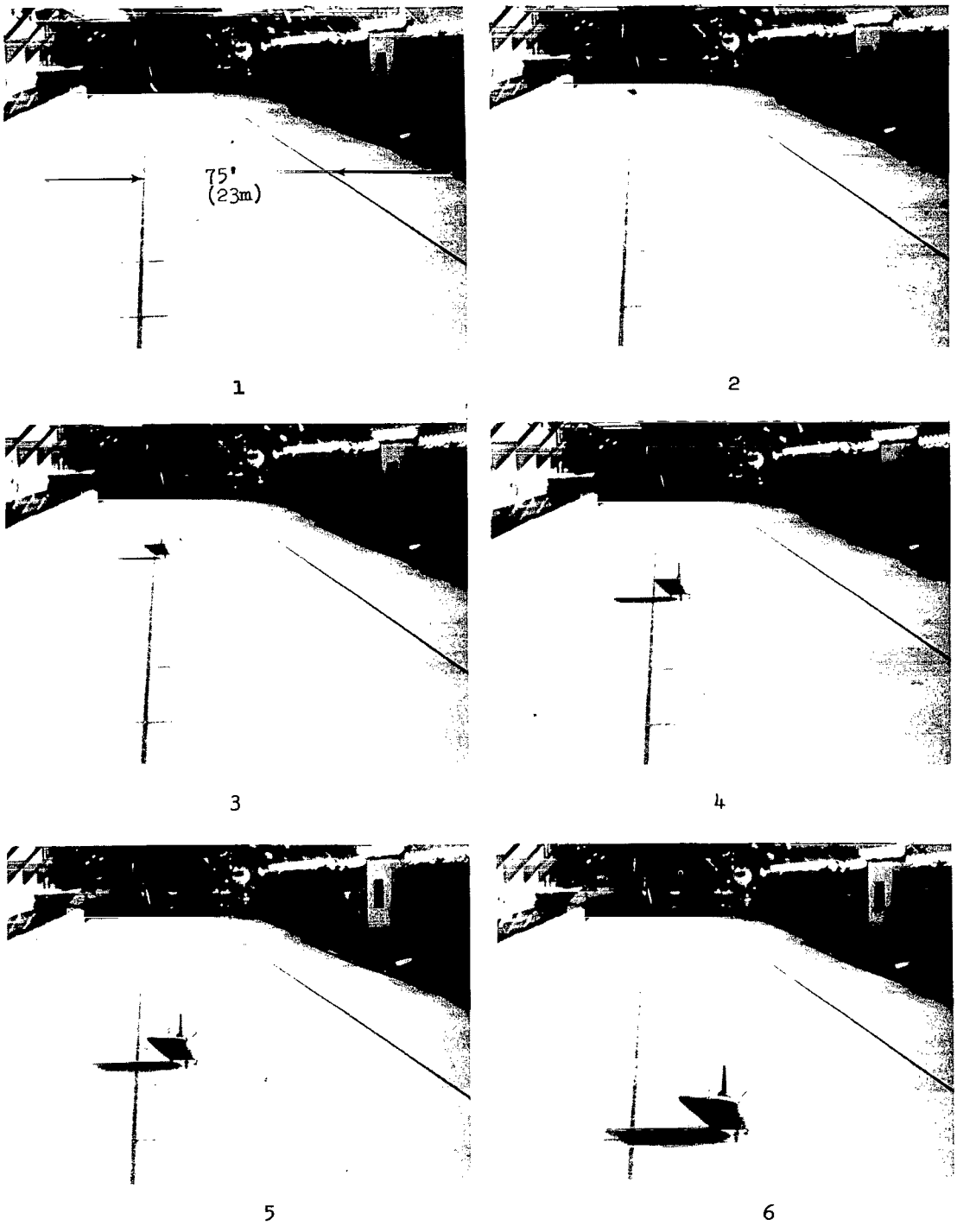

(a) No torque.

L-66-4540

Figure 14.- Typical sequence photographs of slideout tests using the tricycle landing gear showing the effect of torque steering. Vertical velocity, 2 ft/sec (0.6 m/s); horizontal velocity approximately 200 ft/sec (61 m/s); attitude, 0^{0}. (All values are full scale.)

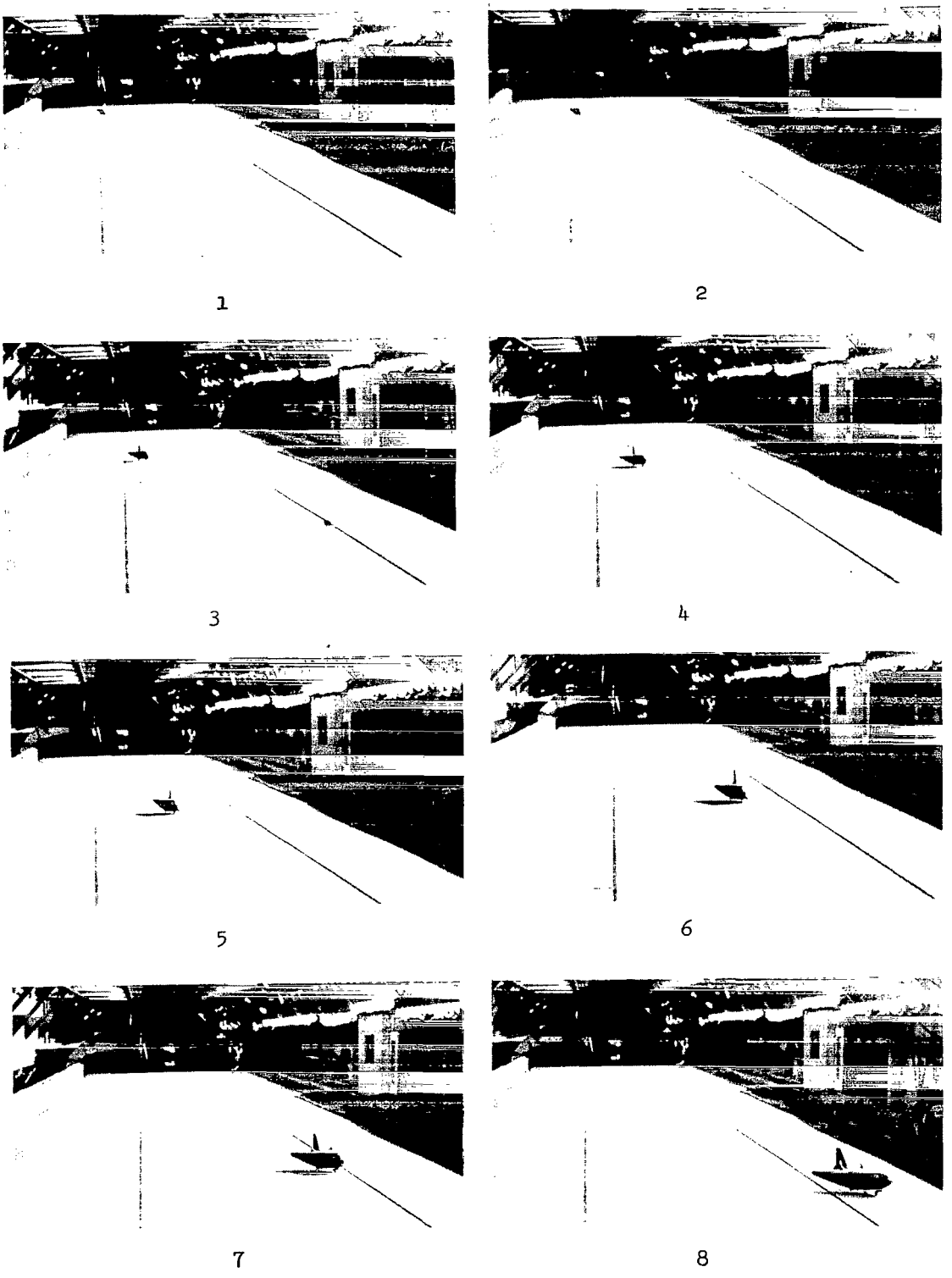

(b) 360 ft-lb (488 m-N) left torque. L-66-4543

Figure 14.- Continued.

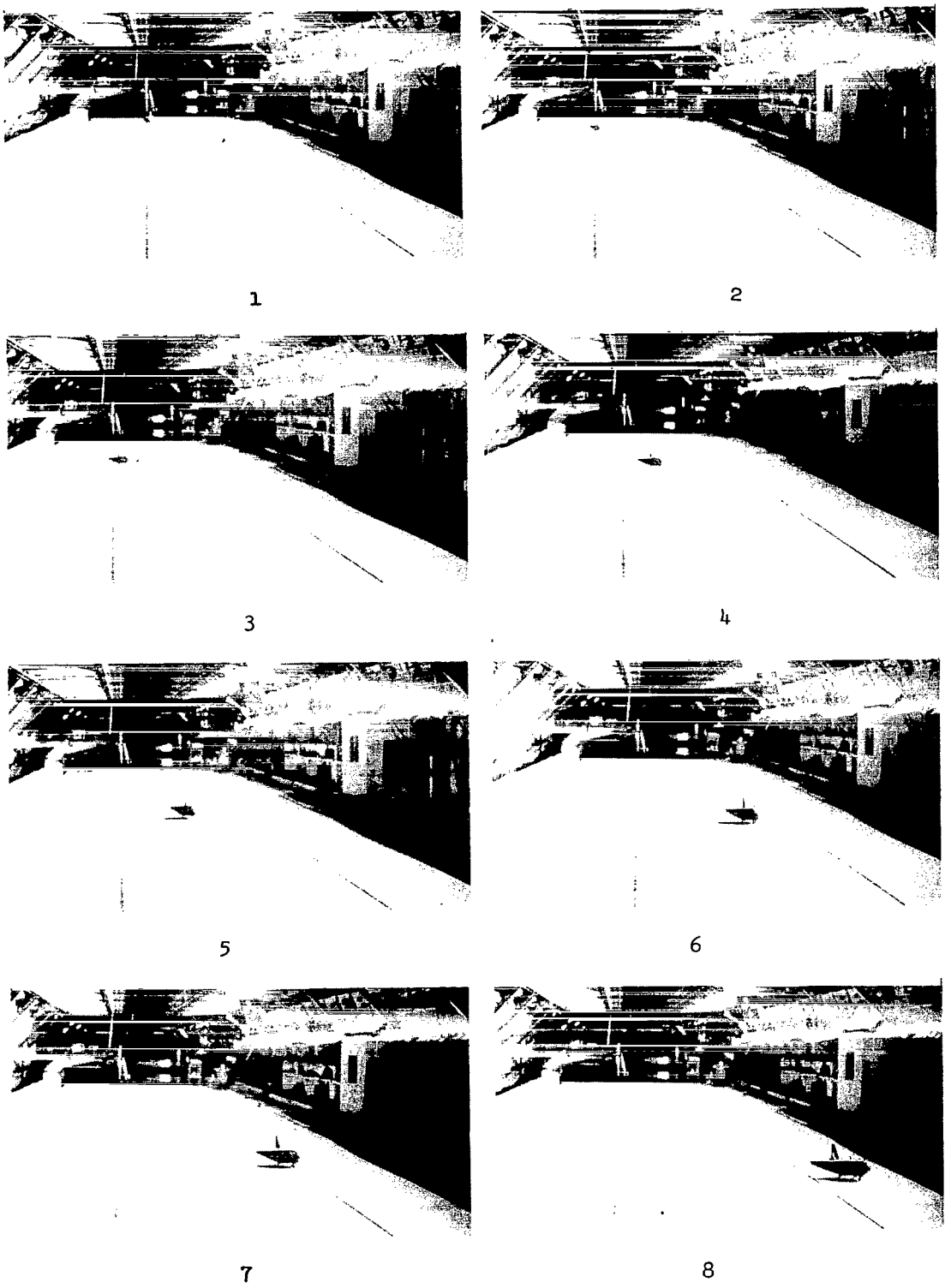

(c) 514 ft-lb (697 m-N) left torque. L-66-4544

Figure 14.- Continued.

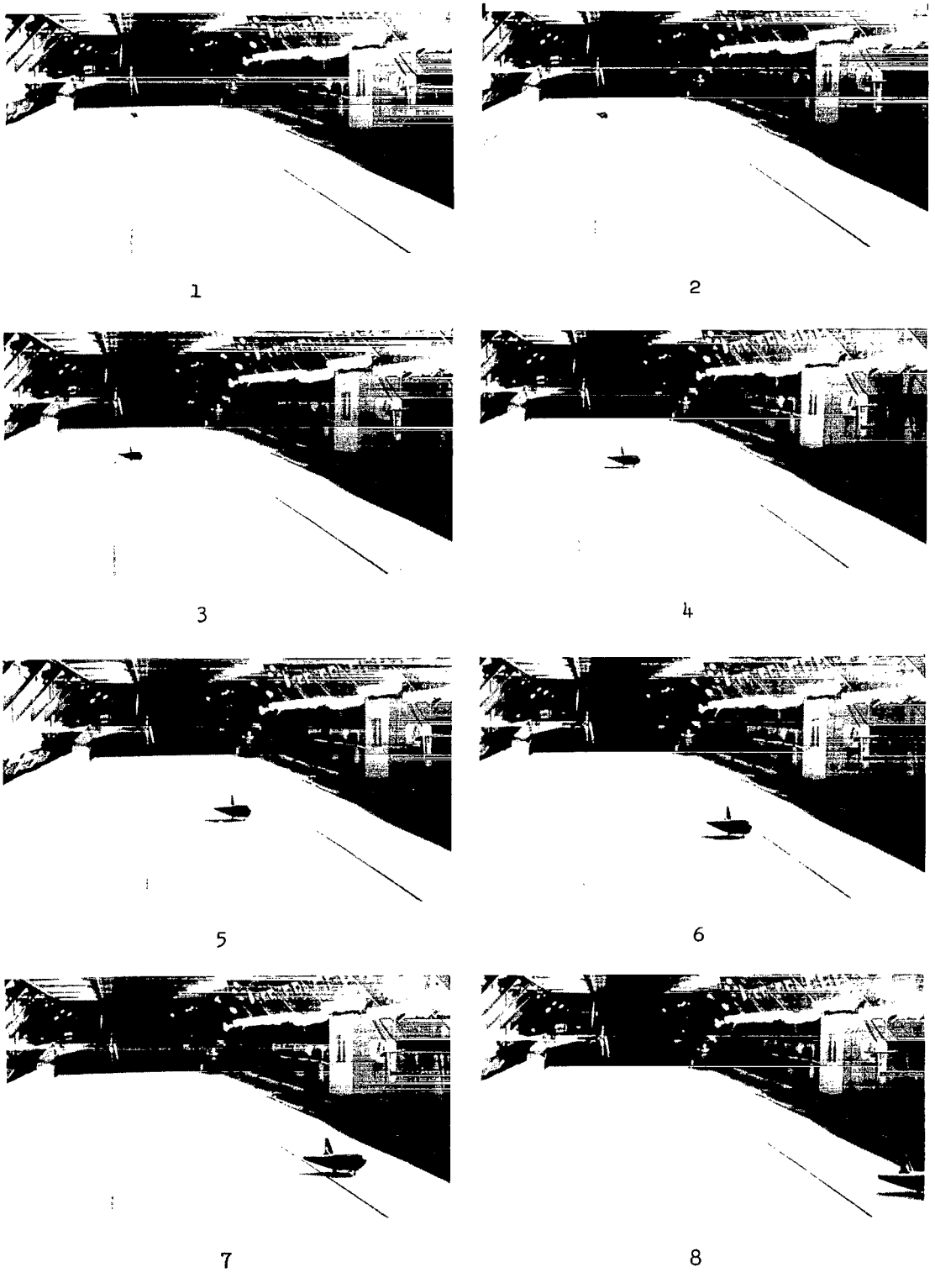

(d) 722 ft-lb (979 m-N) left torque. L-66-4545

Figure 14.- Continued.

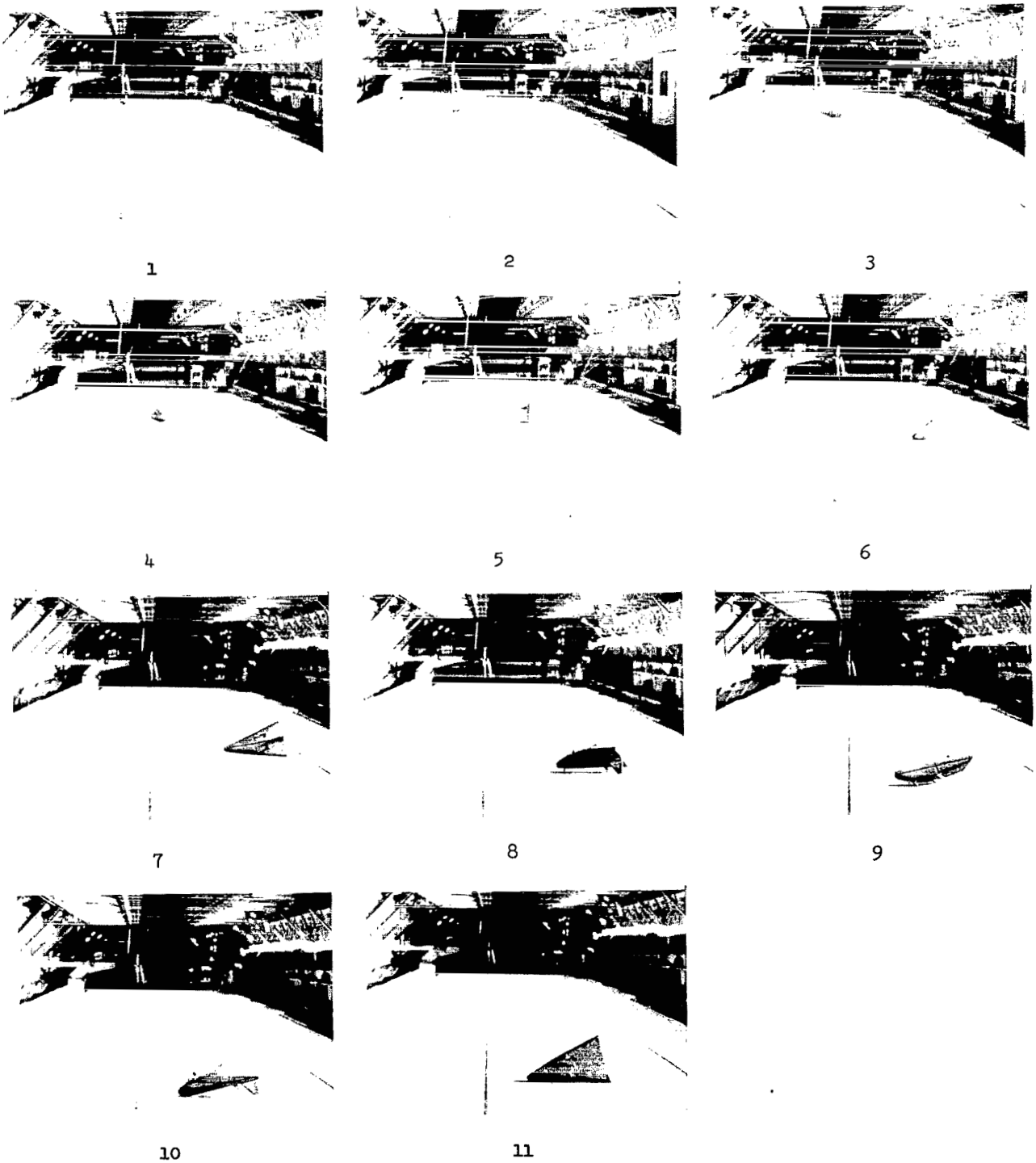

(e) 1029 ft-lb (1395 m-N) left torque. L-66-4546

Figure 14.- Concluded.

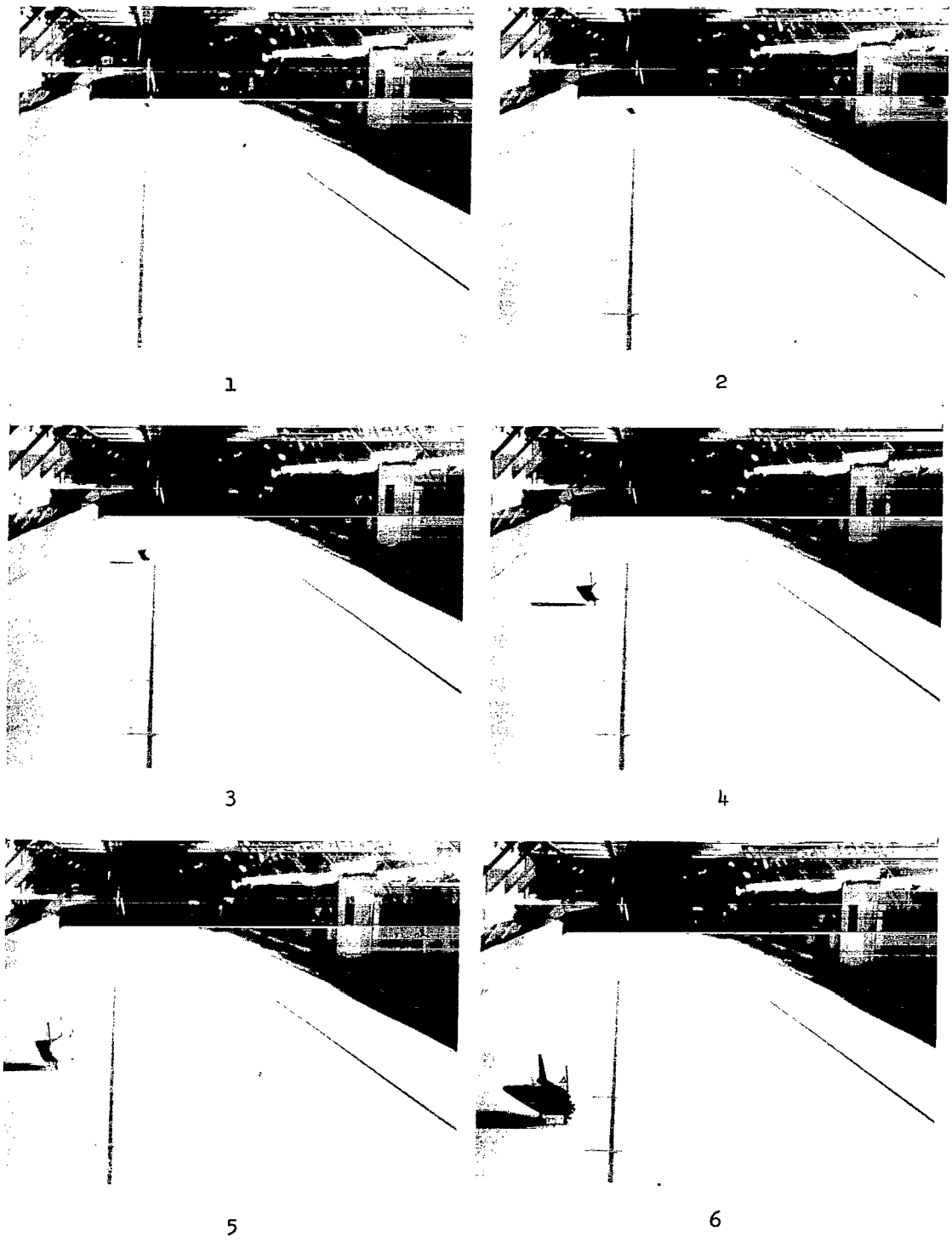

L-66-4547

Figure 15.- Typical sequence photographs of a slideout test with torque steering opposing a right roll. 5^0 roll right, 514 ft-lb (697 m-N) left torque; vertical velocity, 2 ft/sec (0.6 m/s); horizontal velocity, 209 ft/sec (63.7 m/s); attitude, 0^0. (All values are full scale.)

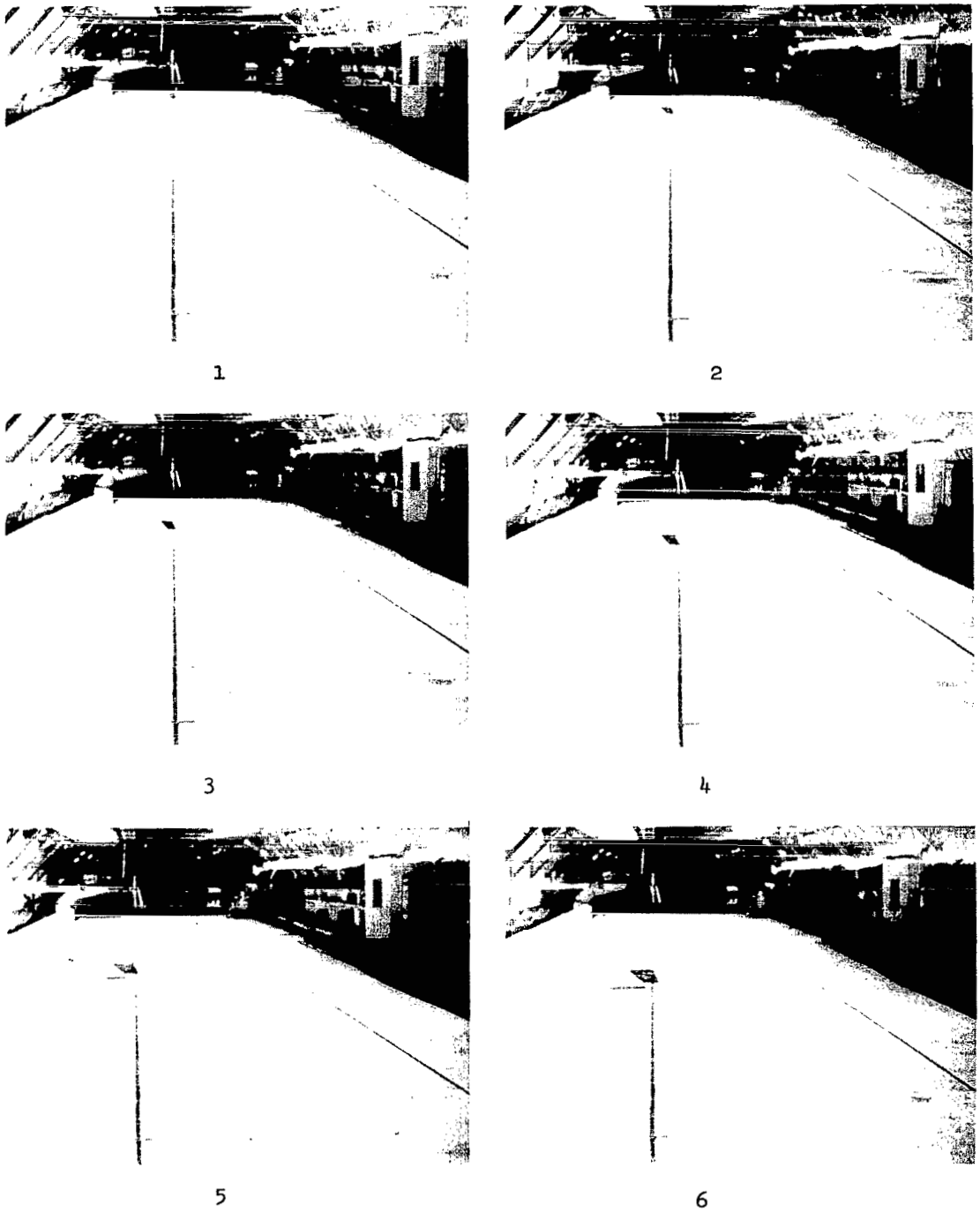

L-66-4548

Figure 16.- Typical sequence photographs of a slideout test using the tricycle landing gear with a nose skid. Vertical velocity, 2 ft/sec (0.6 m/s); horizontal velocity, 196 ft/sec (59.7 m/s); attitude, 0^0; roll left, 5^0. (All values are full scale.)

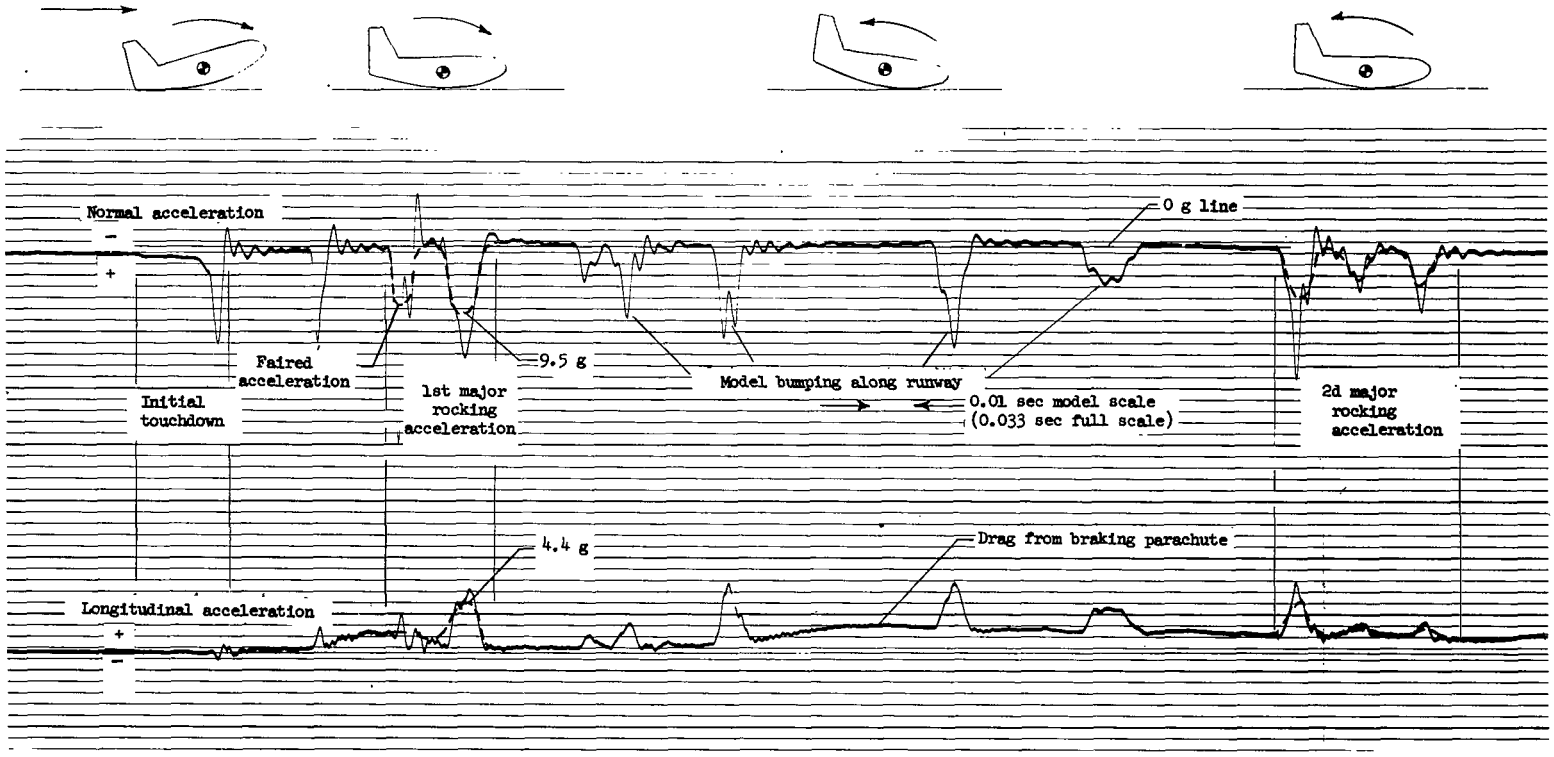

Figure 17.- Typical oscillograph records of the skid-rocker landing configuration for landings made on a plywood runway surface. Vertical velocity, 10 ft/sec (3.0 m/s); horizontal velocity, 325 ft/sec (99 m/s); landing attitude, 15°. (All values are full scale unless otherwise indicated.)

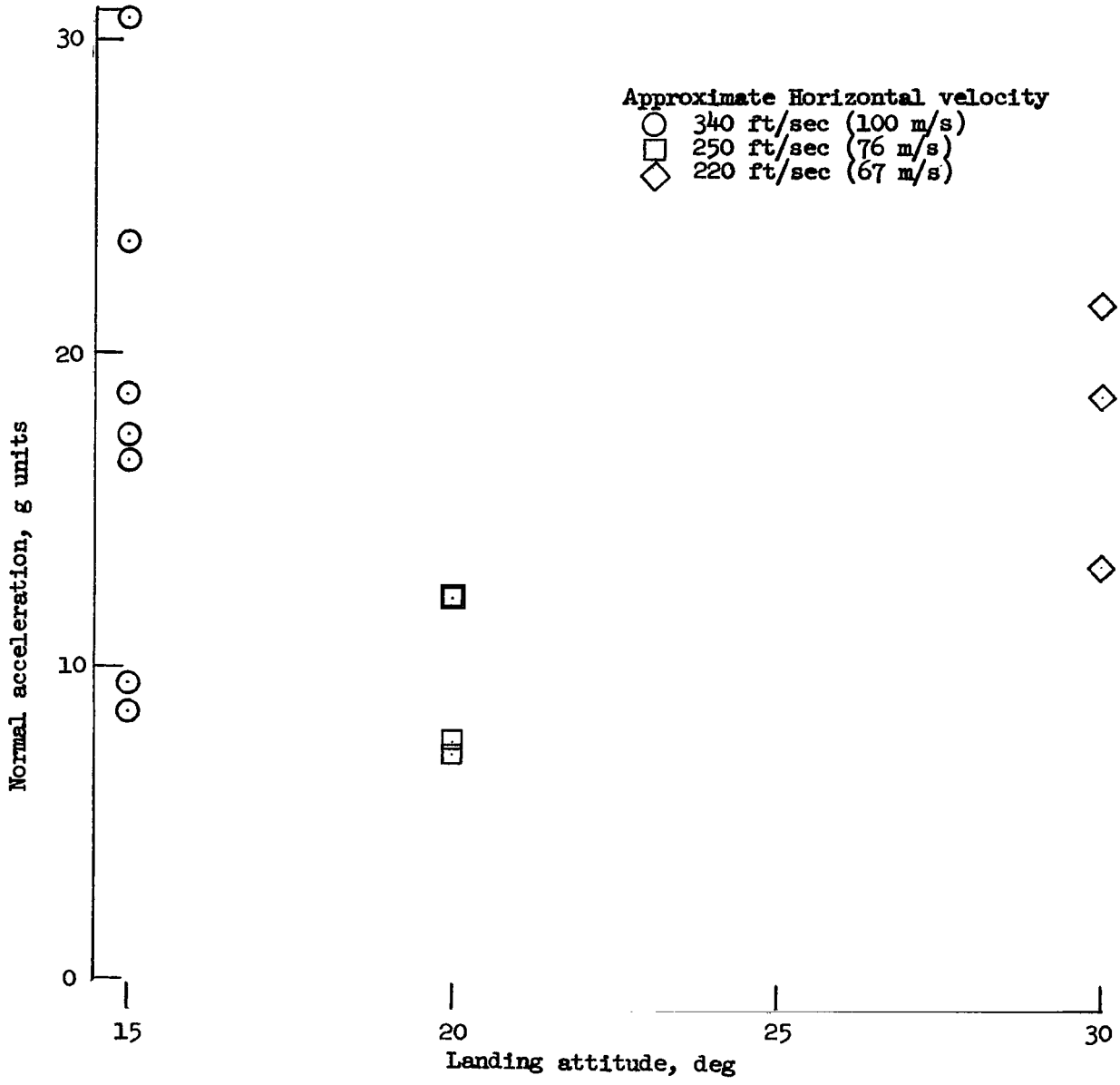

Figure 18.- Maximum normal accelerations for runway-type landings using the skid-rocker configuration with touchdown shock-absorbing tab. Vertical velocity, 10 ft/sec (3.0 m/s). (All values are full scale.)

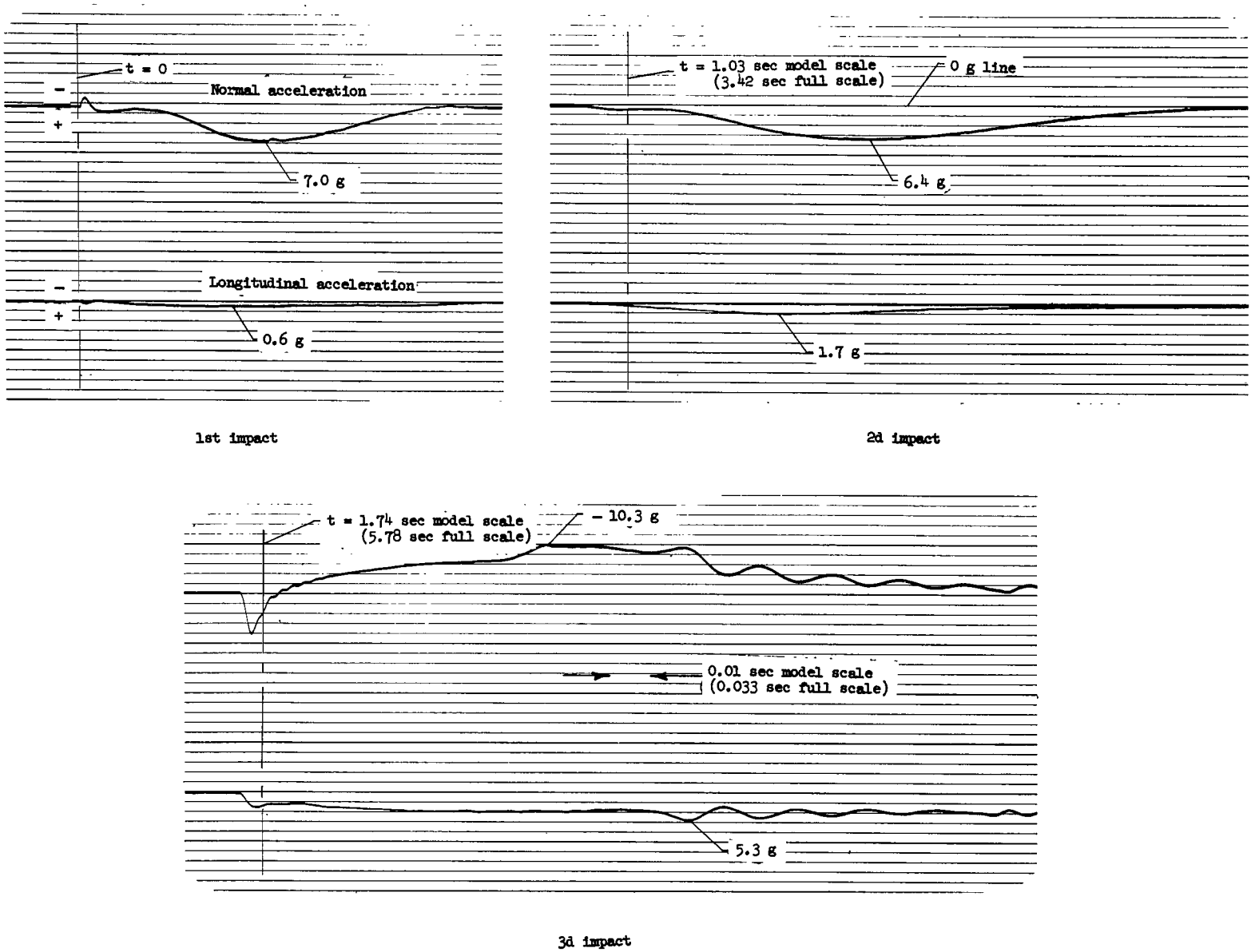

Figure 19.- Typical oscillograph records of accelerations for horizontal landings on calm water. Vertical velocity, 1.5 ft/sec (0.46 m/s); horizontal velocity, 262 ft/sec (79.7 m/s); landing attitude, 25°. (All values are full scale unless otherwise indicated.)

Figure 20.- Vehicle landing in calm water simulating parachute letdown. Vertical velocity, 40 ft/sec (12 m/s); horizontal velocity, 0; attitude, 85°. (All values are full scale.)

L-65-3518

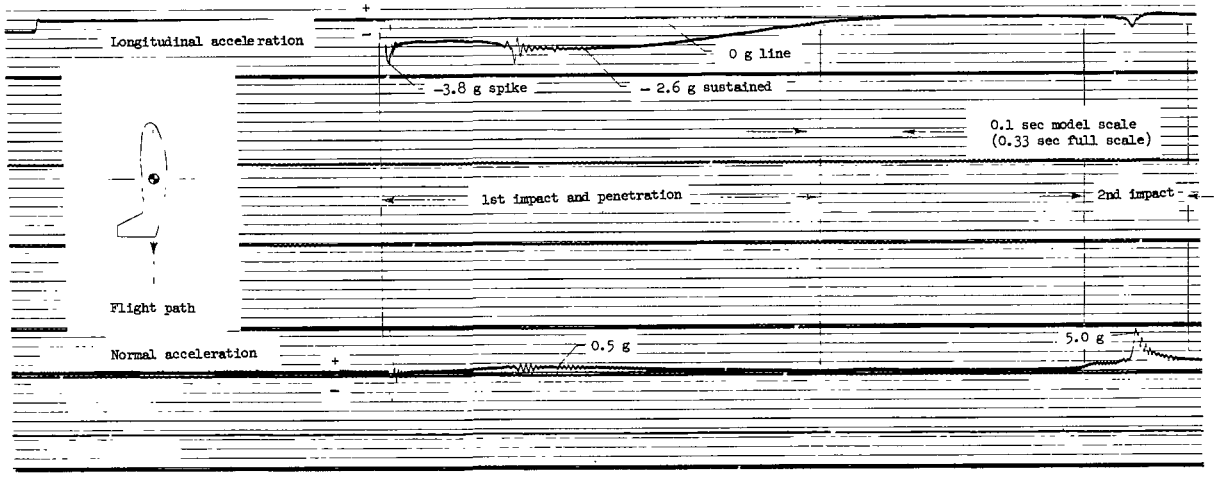

(a) Landing attitude, 90^0.

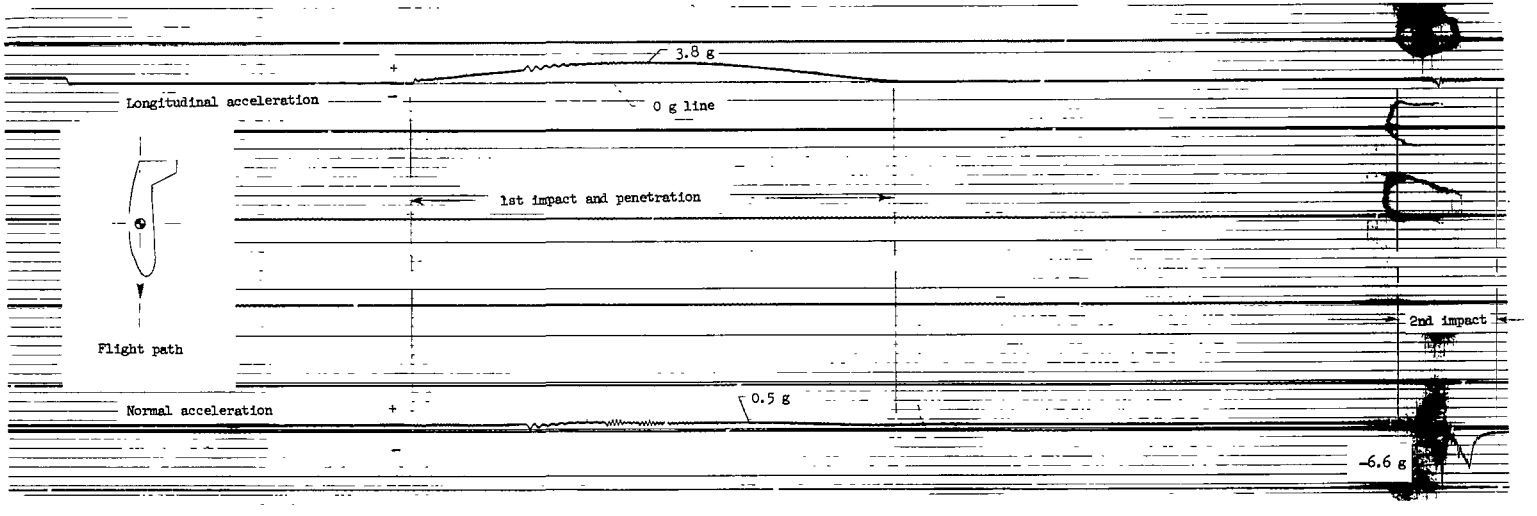

(b) Landing attitude, -90^0.

Figure 21.- Typical oscillograph records of accelerations during vertical landings in calm water. Vertical velocity, 40 ft/sec (12 m/s); horizontal velocity, 0. (All values are full scale unless otherwise indicated.)

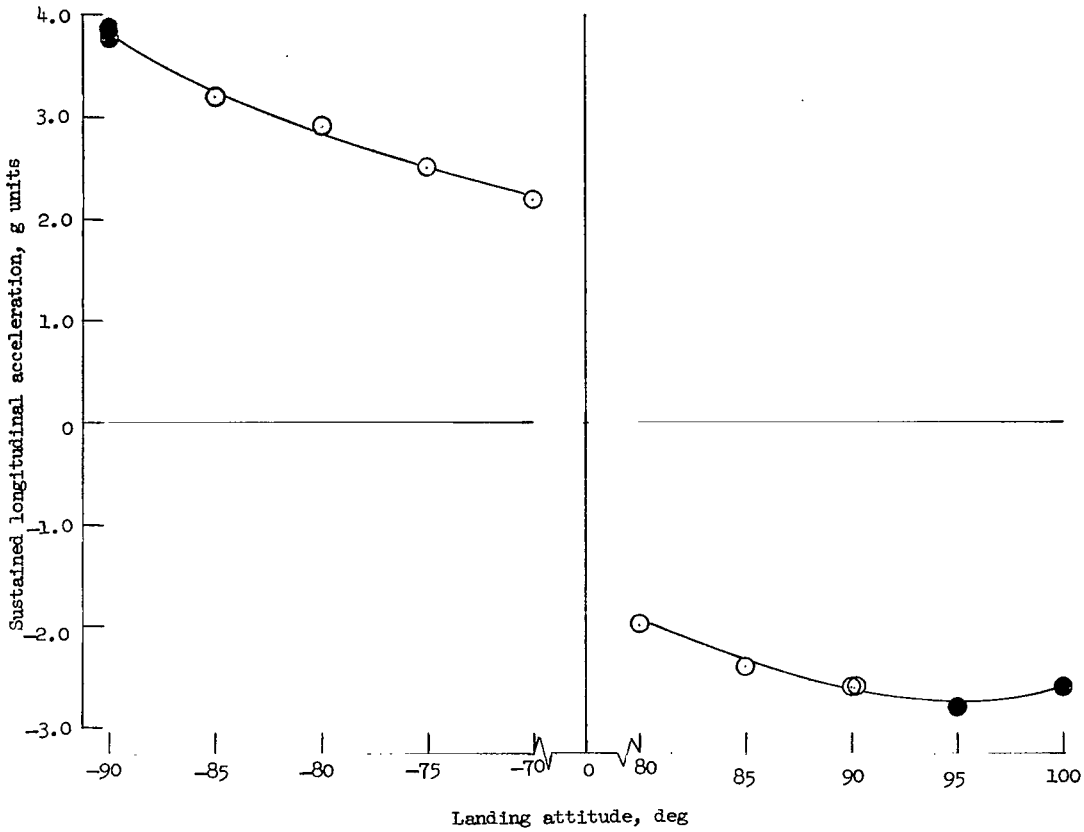

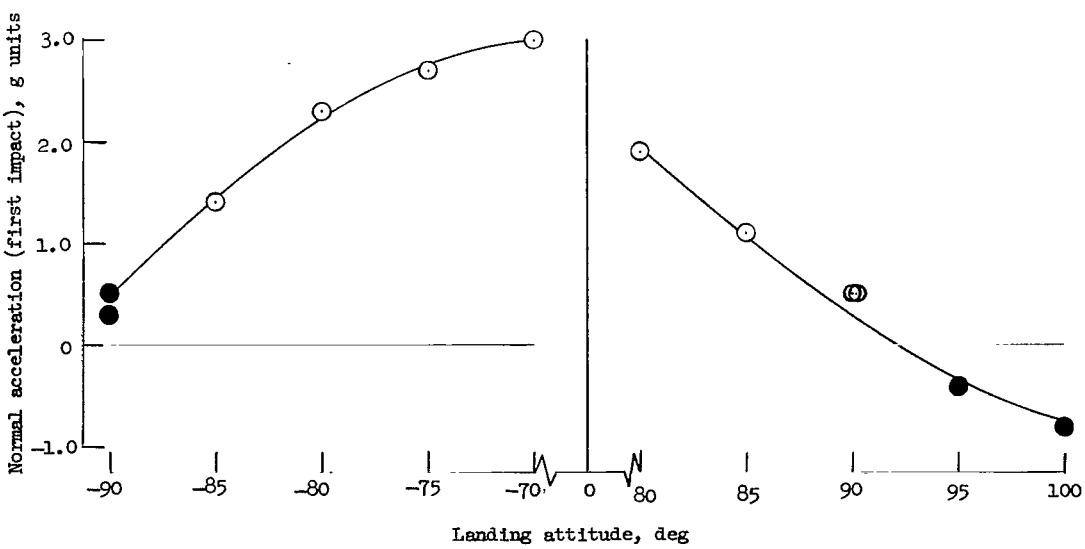

Figure 22.- Longitudinal and normal accelerations for vertical landings in calm water. Vertical velocity, 40 ft/sec (12 m/s); horizontal velocity, 0. Solid symbols indicate the model came to rest in an inverted position.

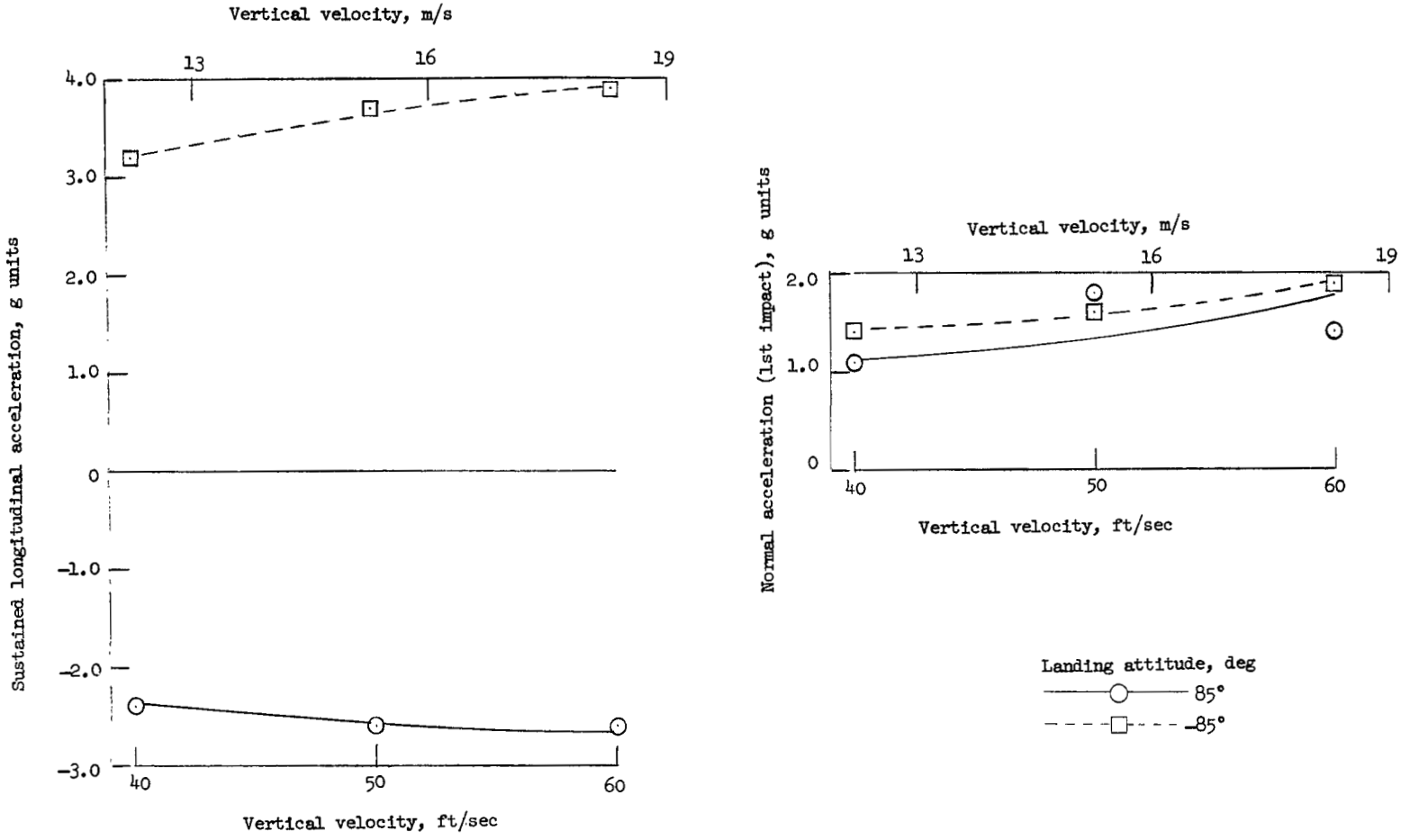

Figure 23.- Effect of increasing vertical velocity on longitudinal and normal accelerations for vertical landings in calm water. Horizontal velocity, 0. (All values are full scale.)

"The aeronautical and space activities of the United States shall be conducted so as to contribute . . . to the expansion of human knowledge of phenomena in the atmosphere and space. The Administration shall provide for the widest practicable and appropriate dissemination of information concerning its activities and the results thereof."

—NATIONAL AERONAUTICS AND SPACE ACT OF 1958

NASA SCIENTIFIC AND TECHNICAL PUBLICATIONS

TECHNICAL REPORTS: Scientific and technical information considered important, complete, and a lasting contribution to existing knowledge.

TECHNICAL NOTES: Information less broad in scope but nevertheless of importance as a contribution to existing knowledge.

TECHNICAL MEMORANDUMS: Information receiving limited distribution because of preliminary data, security classification, or other reasons.

CONTRACTOR REPORTS: Technical information generated in connection with a NASA contract or grant and released under NASA auspices.

TECHNICAL TRANSLATIONS: Information published in a foreign language considered to merit NASA distribution in English.

TECHNICAL REPRINTS: Information derived from NASA activities and initially published in the form of journal articles.

SPECIAL PUBLICATIONS: Information derived from or of value to NASA activities but not necessarily reporting the results of individual NASA-programmed scientific efforts. Publications include conference proceedings, monographs, data compilations, handbooks, sourcebooks, and special bibliographies.

Details on the availability of these publications may be obtained from:

SCIENTIFIC AND TECHNICAL INFORMATION DIVISION

NATIONAL AERONAUTICS AND SPACE ADMINISTRATION

Washington, D.C. 20546